Neurobiology of Aging 80 (2019) 154–172

Contents lists available at ScienceDirect

Neurobiology of Aging

journal homepage: www.elsevier.com/locate/neuaging

Exercise prevents obesity-induced cognitive decline and white matter damage in mice

Leah C. Graham [a,b], Weronika A. Grabowska [a,c], Yoona Chun [a], Shannon L. Risacher [d,e], Vivek M. Philip [a], Andrew J. Saykin [d,e], for the Alzheimer's Disease Neuroimaging Initiative (ADNI)[1], Stacey J. Sukoff Rizzo [a], Gareth R. Howell [a,b,*]

[a] The Jackson Laboratory, Bar Harbor, ME, USA
[b] Sackler School of Graduate Biomedical Sciences, Tufts University School of Medicine, Boston, MA, USA
[c] College of the Atlantic, Bar Harbor, ME, USA
[d] Center for Neuroimaging, Department of Radiology and Imaging Sciences, Indiana University School of Medicine, Indianapolis, IN, USA
[e] Indiana Alzheimer Disease Center, Indiana University School of Medicine, Indianapolis, IN, USA

ARTICLE INFO

Article history:
Received 4 October 2018
Received in revised form 26 March 2019
Accepted 27 March 2019
Available online 3 May 2019

Keywords:
Aging
Brain Health
Obesity
Neuroinflammation
Cerebrovascular Health
Exercise

ABSTRACT

Obesity in the western world has reached epidemic proportions, and yet the long-term effects on brain health are not well understood. To address this, we performed transcriptional profiling of brain regions from a mouse model of western diet (WD)-induced obesity. Both the cortex and hippocampus from C57BL/6J (B6) mice fed either a WD or a control diet from 2 months of age to 12 months of age (equivalent to midlife in a human population) were profiled. Gene set enrichment analyses predicted that genes involved in myelin generation, inflammation, and cerebrovascular health were differentially expressed in brains from WD-fed compared to control diet-fed mice. White matter damage and cerebrovascular decline were evident in brains from WD-fed mice using immunofluorescence and electron microscopy. At the cellular level, the WD caused an increase in the numbers of oligodendrocytes and myeloid cells suggesting that a WD is perturbing myelin turnover. Encouragingly, cerebrovascular damage and white matter damage were prevented by exercising WD-fed mice despite mice still gaining a significant amount of weight. Collectively, these data show that chronic consumption of a WD in B6 mice causes obesity, neuroinflammation, and cerebrovascular and white matter damage, but these potentially damaging effects can be prevented by modifiable risk factors such as exercise.

1. Introduction

Obesity is a major health concern throughout the western world because of its strong association with diseases such as cardiovascular disease, diabetes, and dementias. A western diet (WD) combined with a sedentary lifestyle is the most common cause of weight gain leading to obesity (Campbell, 2004; Cecchini et al., 2010; Cordain et al., 2005), generally characterized by an increased body mass index (BMI) (Calabro et al., 2013; Martin-Rodriguez et al., 2015). Diseases that are influenced by diet and obesity are the greatest cause of morbidity and mortality in the western world, including the United States (World Health Organization, 2009). Health care costs associated with obesity are over $200 billion annually in the United States alone and are ever increasing with 35% of the population classed as obese (Smith and Smith, 2016; Spieker and Pyzocha, 2016).

Cognitive aging is a normal process where structural and functional changes lead to a decline in cognitive ability (Glisky, 2007; Nguyen et al., 2014). However, studies show that obesity and high-fat diets cause cognitive dysfunction in both humans and mice even when controlling for cognitive aging (Elias et al., 2005; Kanoski and Davidson, 2011; Naderali et al., 2009; Pistell et al., 2010). In 1 study that used the word-list learning test (evaluating verbal learning and memory) and the digit symbol substitution test (assessing attention, response speed, and visuomotor coordination), middle aged workers showed a linear association between BMI and cognitive function (Cournot et al., 2006). In a second study, young to aged obese individuals presented poorer executive function than

* Corresponding author at: The Jackson Laboratory, 600 Main Street, Bar Harbor, ME 04660, USA. Tel.: +1 207 288 6572; fax: +1 207 288 6078.
E-mail address: gareth.howell@jax.org (G.R. Howell).

[1] Data used in preparation of this article were obtained from the Alzheimer's Disease Neuroimaging Initiative (ADNI) database (adni.loni.usc.edu). As such, the investigators within the ADNI contributed to the design and implementation of ADNI and/or provided data but did not participate in analysis or writing of this report.

0197-4580/
https://doi.org/10.1016/j.neurobiolaging.2019.03.018

their normal weight counterparts (Gunstad et al., 2007). Obesity and dietary factors also increase risk for dementia—including Alzheimer's disease. One-third of Alzheimer's disease cases, the leading form of dementia globally, is attributed to modifiable risk factors including midlife obesity, physical inactivity, midlife hypertension, and type II diabetes (Norton et al., 2014). These risk factors have also been strongly associated with non-Alzheimer's dementias, including vascular dementia (Nguyen et al., 2014). However, the mechanisms by which high BMI and obesity contribute to cognitive decline and dementias are not understood although inflammation and vascular changes are expected to play an important role (Nguyen et al., 2014).

A WD, midlife obesity, and levels of physical activity (such as aerobic exercise) have direct effects on the structure and function of the brain (Gray et al., 2006; Medic et al., 2016; Tucsek et al., 2014; Veit et al., 2014). Previous studies have shown that diet-induced chronic neuroinflammation and cerebrovascular decline can damage brain structures and reduce cognition (Graham et al., 2016; Montagne et al., 2015; Pistell et al., 2010; Soto et al., 2015, 2016; Valladolid-Acebes et al., 2011). Vascular dysfunction and cerebral small vessel disease are known to increase neuroinflammatory responses, including activation of peripheral and resident myeloid cells (Del Zoppo, 2009; Fornage et al., 2008; Nimmerjahn et al., 2005; Rouhl et al., 2012; Soto et al., 2015; Yang and Rosenberg, 2011). In addition, diet-induced obesity causes systemic inflammation that damages the microvasculature of the brain in aging and dementia (Grammas et al., 2006; Grammas and Ovase, 2001). Some studies have correlated high BMI and cerebrovascular damage with lower gray matter volume and changes to white matter density in humans (Kalaria, 2010; Medic et al., 2016; Veit et al., 2014). Together, systemic inflammation and cerebrovascular changes, induced by diet and/or obesity, are likely key drivers of cognitive decline and a predisposition for dementia. However, the precise relationships between diet-induced obesity, neuroinflammation, and brain structure/function are not known.

Increased risk of age-related cognitive decline and dementia due to poor diet and obesity is often coupled with physical inactivity. Exercise can ameliorate disease onset and progression in some individuals, independent of diet and obesity (Duncan et al., 2003; Gaesser et al., 2014; Lee et al., 2005). For instance, studies have shown a reduced rate of cognitive decline and a decreased incidence of Alzheimer's disease in active older adults (Kalaria, 2010; Lautenschlager et al., 2008; Mattson, 2012; Rovio et al., 2010). Exercise can reduce age-related brain tissue loss and stimulate neurogenesis in the hippocampus (HP) (Colcombe et al., 2003; Nokia et al., 2016; Van Praag et al., 2005), but a detailed analysis of the positive effects of exercise on the brain in chronic obesity has not been performed.

In this study, we set out to identify the effects of chronic obesity from young to midlife on brain health. Unbiased transcriptional profiling of the HP, cortex, and corpus callosum from WD-fed mice compared to chow-fed mice identified expression changes in genes and pathways involved in neuroinflammation, vasculature, and myelination. Histologically, the greatest alterations were observed to white matter regions where cerebrovascular dysfunction preceded myelin phagocytosis by myeloid cells and age-dependent cognitive decline. Importantly, exercise prevented obesity-induced white matter damage by suppressing neuroinflammation and vascular dysfunction despite significant weight gain.

2. Materials and methods

2.1. Animals

All methods are in accordance with The Jackson Laboratory Institutional Animal Care and Use Committee (IACUC)–approved protocols. C57BL/6J (B6) (JAX stock # 000664) male mice were used exclusively in this study to avoid effects of the estrus cycle in female mice. Data show the estrus cycle greatly impacts the effects of high-fat diet. In 1 study, postwean high-fat diet feeding caused irregular estrus cycles and increases in leptin in 30% of female mice (Lie et al., 2013). In a second study, a high-fat diet caused complete acyclicity including elongation of phases, skipping of phases, or a combination of both (Chakraborty et al., 2016). Changes in the estrus cycle are known to affect cognitive ability (Broestl et al., 2018; Markowska, 1999). These estrus-dependent variables would confound the results of this initial study to understand the effects of a WD on brain health. Follow-up studies will be required to determine the similarities or differences between male and female mice.

All male mice were maintained on a 12/12 hours light/dark cycle. For running experiments, mice were given free access to running saucer wheels (Innovive Inc). Sedentary mice had no access to running wheels. Cohorts were maintained from wean on standard LabDiet 5K52 (referred to as control or normal chow diet). Half of the mice in the sedentary and running cohorts were switched to TestDiet 5W80 (WD) adapted from TestDiet 5TLN with added high-fructose corn syrup, lower fiber, and increased milk protein and fat (Graham et al., 2016) at 2 months of age to avoid changes to brain development (Fig. S1A). Data collected for food intake were assessed everyday for 15 days when mice were 10 months of age (mos). Daily monitoring of mice via routine health care checks was carried out to determine their general well-being. Approximately 10% of mice fed the WD developed dermatitis and were eliminated from this study using an IACUC-approved CO_2 euthanasia protocol. A timeline describing the timing of WD, behavioral assays, harvesting, and running wheels for each experiment is provided (Fig. S1B).

2.2. Assessment of running distance

Animals were tested for running capacity by placing individual mice in a cage with a wireless saucer wheel (ENV-044 Med Associates Inc) for 15 days. Data were collected nightly (16 hours) and analyzed, and average distance ran per night/mouse was calculated.

2.3. Behavioral battery

The Jackson Laboratory's Mouse NeuroBehavioral Facility performed the behavioral tasks, with the exception of nest construction and burrowing that were assessed in the Howell laboratory as reported previously (Deacon, 2012). All Mouse NeuroBehavioral Facility tasks were previously validated using control mice. Importantly, all technicians were blind to treatment and age during testing and until after the data analysis was complete. The test order of subjects was randomized and counterbalanced across multiples of sessions and equipment.

For grip strength, subjects were weighed and acclimated for at least 1 hour before the test. Grip strength was assessed using the Bioseb grip strength meter (Model# BIO-GS3 Bioseb, Inc, Vitrolles, France) equipped with a grid suited for mice (100 × 80 mm, angled 20°). For forepaw and 4-paw grip strength testing, mice were lowered toward the grid by their tails to allow for visual placing and for the mouse to grip the grid with their paws. Subjects were firmly pulled horizontally away from the grid (parallel to the floor) for 6 consecutive trials with a brief (<30 seconds) rest period on the bench between trials. Trials 1–3 tested only the forepaw grip, whereas trials 4–6 included all 4 paws. The average of the 3 forepaw trials and the average of the 3 four-paw trials were analyzed with and without normalization for body weight.

For assessment of open field activity, Open Field Arenas (40 cm × 40 cm × 40 cm; Omnitech Electronics, Columbus, OH)

were used. A light fixture mounted ~50 cm above the center of each arena provided a consistent illumination of ~400–500 lux in the center of the field. Before the test, mice were acclimated to an anteroom outside the testing room for a minimum of 1 hour. Subsequently, the tested mice were placed individually into the center of the arena where the infrared beams recorded distance traveled (cm), vertical activity, and perimeter/center time.

The spontaneous alternation task was conducted as previously described (Sukoff Rizzo et al., 2018). Briefly, a clear polycarbonate arena in the shape of a Y (fabricated in-house at The Jackson Laboratory) with identical arm dimensions (33.65 cm length, 6 cm width, 15 cm height) with a removable aerated lid and no intended visual cues were used under adjusted, ambient lighting (~50 lux). Subject mice were acclimated to the testing room for 1 hour before testing. Subjects were then placed midway of the start arm (A), facing the center of the Y for an 8-minute test period, and the sequence of entries into each arm was recorded via a ceiling mounted camera integrated with behavioral tracking software (Noldus EthoVision). The percentage of spontaneous alternation was calculated as the number of triads (entries into each of the 3 different arms of the maze in a sequence of 3 without returning to a previously visited arm) relative to the number of alteration opportunities. Re-entries were allowed and so chance was considered 22%.

For novel spatial recognition, a y-shaped arena, similar to the arena described for the spontaneous alternation task, was used. For this task, distinct visual cues were placed at the distal end of each arm (see Sukoff Rizzo et al., 2018 for detailed methods and visual cue information). During trial 1, only 2 of 3 arms were accessible for a 10-minute period, whereas during trial 2, which occurred after a 30-minute delay period in which subjects were returned to their home cages, all arms were accessible and subjects were allotted a 5-minute exploration period. Intact memory in this assay was indicated by a preference for spending time in the novel arm (>33%).

2.4. Mouse perfusion and tissue preparation

Tissues were collected at 3.5 and 12 months. Mice were anesthetized with a lethal dose of ketamine/xylazine, transcardially perfused with 1X phosphate buffered saline (PBS), and brains carefully dissected and hemisected in the midsagittal plane. One half was snap-frozen, and the other half was immersion-fixed in 4% paraformaldehyde for 2 nights at 4 °C. After fixation, brains were rinsed in 1X PBS, immersed on 30% sucrose/PBS overnight at 4 °C, frozen in OCT, and cryosectioned at 25 μm.

2.5. RNA and protein extraction with TRIzol, library construction, sequencing, and analysis

For RNA-seq, brains were dissected as described previously and the superior region of the cortex containing the frontal parietal cortex/corpus callosum (FPC/CC) and the HP were extracted and snap-frozen at the time of collection and stored at −80 °C. RNA extraction was performed according to the TRIzol (Invitrogen, cat #: 15596026) manufacturer's instructions and as described in previous publications from our laboratory (Soto et al., 2015). Total RNA was purified from the aqueous layer using the QIAGEN miRNeasy mini extraction kit (QIAGEN) according to the manufacturer's instructions. RNA quality was assessed with the Bioanalyzer 2100 (Agilent Technologies). Poly(A) selected RNA-seq sequencing libraries were generated using the TruSeq RNA Sample preparation kit v2 (Illumina) and quantified using qPCR (Kapa Biosystems). Using Truseq V4 SBS chemistry, all libraries were processed for 125 base pair (bp) paired-end sequencing on the Illumina HiSeq 2500 platform according to the manufacturer's instructions. Each sample was subjected to quality control step using NGSQCToolkit v2.3 for the removal of adapters and trimming low-quality bases (Phred <30) (Patel and Jain, 2012). Next, we used RSEM v1.2.12 to quantify gene expression using the trimmed reads as input (Li and Dewey, 2011). RSEM internally uses Bowtie2 as its aligner (Langmead et al., 2009). Following alignment and expression quantification, differential gene expression analysis was performed per brain region, using edgeR v2.6.10 (Robinson et al., 2010). We applied a filtering step to remove genes with low expression by removing any gene that did not have at least 1 read per million for at least 2 samples. After filtering, trimmed mean of M values normalization was applied to remove any potential library size biases. Specifically, for the comparisons of diets, we assessed differences in gene expression between chow and WD, whereas for the comparison of age, we performed all pairwise comparisons of ages 3.5 months and 10 months as well as chow and WD. In all comparisons, genes were defined as significantly differential expression at FDR <0.05. Differentially expressed (DE) genes for specific comparisons are provided (Tables S1–4) and raw RNA-sequencing data will be made available on GEOarchive (Gene Expression Omnibus Archive).

2.6. RNA in situ hybridization

For in situ hybridization, an RNA probe for mouse *Plp* (GE Dharmacon Clone ID: 5364736) was synthesized, labeled with digoxigenin (Dig), and hydrolized. Frozen sections were postfixed (4% paraformaldehyde for 5 minutes), rinsed twice with 1X PBS, and acetylated with 0.25% acetic anhydride for 10 min in 0.1 M triethanolamine. Sections were then washed in PBS and incubated overnight at 65 °C in hybridization solution [50% formamide, 1X Hybe solution (Sigma-Aldrich), 1 mg/mL yeast RNA] containing 1 g/mL Dig-labeled riboprobe. After hybridization, sections were washed by immersion in 0.2X saline-sodium citrate buffer at 72 °C for 1 hour. Dig-labeled probes were detected with an AP-conjugated anti-Dig antibody (Roche) followed by NBT/BCIP (nitroblue tetrazolium/5-bromo-4-chloro-3-indolyl phosphate) reaction (Roche). After in situ hybridization, sections were incubated with DAPI for nuclei staining and mounted in Aqua-Poly/Mount (Polysciences) as described previously (Howell et al., 2011). Images taken of *Plp* in situ hybridization were obtained using a Nikon Eclipse E200 microscope using SPOT Basic 5.2 imaging software.

2.7. Immunofluorescence

For immunostaining with antibodies against vascular associated proteins, sections were pretreated with pepsin as previously described (Franciosi et al., 2007) with minor modifications. Sections were hydrated with H_2O for 3 minutes (min) at 37 °C followed by treatment of the tissue with 0.5 mg/mL of Pepsin (Sigma) for 18 minutes at 37 °C. Sections were then rinsed twice with 1X PBS at room temperature for 10 minutes. After pepsin pretreatment, sections were rinsed once in 1X PBT (1% PBS +1% Triton 100X) and incubated in primary antibodies: goat anti-PDGFRβ (1:40, R&D), goat anti-CD31 (1:40, R&D), rabbit anti-LAM (1:200, Sigma-Aldrich) diluted in 1X PBT +10% normal goat or normal donkey serum for 2 nights at 4 °C. Secondary antibody protocols identical to that used for nonvascular associated protein immunofluorescence were followed (see the following).

Sections used for nonvascular associated protein visualization were dried for 15 min at 37 °C followed by one 10-minute wash in 1X PBT (1% PBS +1% Triton 100X) at room temperature and incubated in primary antibodies: chicken anti-GFAP (1: 200, Acris), rabbit anti-GFAP (1:200, Dako), rabbit anti–myelin basic protein (MBP; 1:200, Abcam), rat anti-MBP (1:200, Abcam), goat anti-IBA1 (1:100, Abcam), rabbit anti-IBA1 (1:100, Wako), rat anti-CD68

(1:100, Bio-Rad), goat anti-OLIG2 (1:100, R&D Systems), and mouse anti-APC (CC-1, 1:50, Millipore) diluted in 1X PBT + 10% normal goat or normal donkey serum for 2 nights at 4 °C. After incubation with primary antibodies, all sections were rinsed 3 times with 1X PBT for 10 minutes and incubated for 2 hours in the corresponding secondary antibodies (1:1000, Invitrogen). Tissue was then washed 3 times with 1X PBT for 10–15 minutes, incubated with DAPI for 5 min, and mounted in Aqua-Poly/Mount (Polysciences).

2.8. Imaging and quantification

2.8.1. Imaging

For each mouse, 4 images per brain region (parietal cortex, corpus callosum, and CA1 region of the HP) were generated. For quantifying cell number or area, images were captured on a Zeiss AxioImager microscope. For quantification in IMARIS 8.1 (Bitplane), images were captured on the Leica SP5 confocal microscope. Z stacks were compiled with 0.20 μm steps in the z direction with 1024 × 1024 pixel resolution. For each antibody, all images were captured using identical parameters for accurate quantification. Where possible, fluorescent intensity was standardized to samples from chow-fed mice. However, given the striking difference in intensity between chow-fed and WD-fed mice for MPB, images were standardized to WD-fed mice.

2.8.2. Quantification in FIJI

Images for GFAP+, IBA1+, MBP+, CD68+, Olig2+, CC-1+ cells were manually counted using the cell counter plugin for FIJI v1.0. For quantification of PDGFRβ, Laminin, and CD31, fluorescent area was calculated using a previously validated in-house Vascular Network Toolkit plugin for FIJI v1.0 (Soto et al., 2015) (see Statistical Analyses section). Investigators were blinded for all quantifications including cell counts and cell/protein area.

2.8.3. Quantification and visualization in IMARIS

Images were rendered using identical parameters, and the colocalization tool was used to determine both the surface areas of MBP, IBA1, and CD68 and the interactions between surfaces.

2.9. Western blot analysis

Protein samples were separated by SDS-PAGE gel electrophoresis and transferred to nitrocellulose membrane. Before incubation with primary antibodies, membranes were blocked in 5% non–fat-dried milk diluted in 0.1% PBS-Tween, and after primary antibody incubation, the appropriate peroxidase-conjugated antibody (Millipore) was used as a secondary antibody. For detection, membranes were treated with the Amersham ECL western blotting analysis system (GE Healthcare) and exposed to the High performance chemiluminescence film (GE Healthcare). The primary antibodies used for immunoblotting are as follows: rat anti-Myelin Basic Protein (predicted band sizes: 19 and 26 kDa, MBP, 1:1,000, Abcam) and rabbit anti-β Actin (1:1,000, Abcam).

2.10. Transmission electron microscopy

Mouse perfusion and brain sectioning were performed as previously reported (Soto et al., 2015). Grids were viewed on a JEOL JEM1230 transmission electron microscope, and images were collected with an AMT high-resolution digital camera. Ten to 20 images per brain/mouse were taken with n = 5 per group (young chow, and 12 months WD and chow). G-ratio was calculated by determining the ratio of the inner axonal radius and the outer axonal radius (Chomiak and Hu, 2009; Rushton, 1951). At least 200 myelinated axons were measured in the corpus callosum of 3.5-month chow, 12-month chow, and 12-month WD mice (n = 3 mice).

2.11. Human imaging studies

Participants from the Alzheimer's Disease Neuroimaging Initiative (ADNI) were used in this study to evaluate whether white matter changes associated with obesity were seen in older adults with and without cognitive impairment. ADNI was launched in 2003 by the National Institute on Aging, the National Institute of Biomedical Imaging and Bioengineering, the Food and Drug Administration, private pharmaceutical companies, and non-profit organizations as a $60 million, 5-year public-private partnership. The primary goal of ADNI has been to test whether serial magnetic resonance imaging, positron emission tomography, other biological markers, and clinical and neuropsychological assessment can be combined to measure the progression of mild cognitive impairment (MCI) and early Alzheimer's disease. Determination of sensitive and specific markers of very early Alzheimer's disease progression is intended to aid researchers and clinicians to develop new treatments and monitor their effectiveness, as well as lessen the time and cost of clinical trials.

The principal investigator of this initiative is Michael W. Weiner, MD, the VA Medical Center, as well as the University of California-San Francisco. ADNI is the result of efforts of many coinvestigators from a broad range of academic institutions and private corporations, and subjects have been recruited from over 50 sites across the United States and Canada. The initial goal of ADNI was to recruit 800 subjects but ADNI has been followed by ADNI-GO and ADNI-2. To date, these 3 protocols have recruited over 1500 adults, ages 55 to 90, to participate in the research, consisting of cognitively normal older individuals, people with early or late MCI, and people with early Alzheimer's disease. The follow-up duration of each group is specified in the protocols for ADNI-1, ADNI-GO, and ADNI-2. Subjects originally recruited for ADNI-1 and ADNI-GO had the option to be followed in ADNI-2. Further information can be found at http://www.adni-info.org/ and in previous reports (Jack et al., 2010; Jagust et al., 2010; Petersen et al., 2010; Saykin et al., 2010; Trojanowski et al., 2010; Weiner et al., 2010). Informed consent was obtained according to the Declaration of Helsinki.

Participants in this study were included if they had diffusion tensor imaging (DTI) at baseline, as well as concurrent weight and height measurements to calculate BMI, demographics, and medical history data (n = 256). Participants included 88 cognitively normal (CN) older adults, 120 patients with MCI, and 48 participants with mild Alzheimer's disease. BMI was calculated using the standard formula and participants were divided into obese (BMI > 30) and nonobese (BMI ≤ 30). Medical history pertaining to cardiovascular disorders was extracted from the medical history database through manual inspection and participants were classified as yes or no for having a history of atrial fibrillation, cardiac arrhythmia, cardiac bypass surgery, cardiac surgery other than a cardiac bypass surgery, chronic obstructive pulmonary disease, diabetes, hypertension, hyperlipidemia, sleep apnea, smoking, or transient ischemic attack or stroke.

Preprocessed DTI scans were downloaded from the ADNI data repository (http://adni.loni.usc.edu/). Scans were preprocessed using standard techniques as previously described, including Eddy-current correction, masking, spatial normalization, fitting of diffusion tensor models, and coregistration to standard space in FSL (http://fsl.fmrib.ox.ac.uk/fsl/fslwiki/). Specifically, corrected fractional anisotropy (FA), mean diffusivity (MD), radial diffusivity (RD), and axial diffusivity (AD) scans were downloaded. For reference, FA is a general measure of white matter integrity, while measures of diffusivity provide more specific information about the white

matter tracts (Alexander et al., 2007). In particular, RD with relatively unchanged AD has been shown to be a marker of dysmyelination (Song et al., 2002). In addition, region of interest data from the LONI site, processed by ADNI investigators using the Enhancing Neuro Imaging Genetics through Meta-Analysis (ENIGMA) protocol (http://enigma.loni.usc.edu/wp-content/uploads/2012/06/ENIGMA_TBSS_protocol.pdf), were downloaded. Regional measures for all DTI scalars (FA, MD, RD, AD) in the corpus callosum were then assessed for differences between nonobese and obese individuals. Diabetes history was the only medical history variable from the list mentioned previously that was significantly associated with corpus callosum scalar measures, and only in the full sample. Thus, in the final models, the residual scalar measures adjusted for age, sex, diabetes history, and diagnosis (CN, MCI, AD) for the full sample (n = 256) and residuals adjusted for age and sex for the CN participants only (n = 88) were evaluated for differences between groups using a two-sample *t*-test in SPSS version 24.0.

Finally, corrected FA, MD, RD, and AD scans were analyzed using tract-based spatial statistics (http://fsl.fmrib.ox.ac.uk/fsl/fslwiki/TBSS; Smith et al., 2006), part of FSL. First, FA images were created by fitting a tensor model to the raw diffusion data using FDT and then brain-extracted using BET (Smith, 2002). All subjects' FA data were then aligned into a common space using the nonlinear registration tool FNIRT, which uses a b-spline representation of the registration warp field. Next, the mean FA image was created and thinned to create a mean FA skeleton, which represents the center of all tracts common to the group. Each subject's aligned FA data were then projected onto this skeleton and the resulting data fed into voxelwise cross-subject statistics. Specifically, regions where nonobese and obese participants differed were analyzed using the same covariates as in the regional analysis. Analyses were done both in all participants and in CN only. However, results were very similar, and thus, only the voxelwise results for all participants are shown for simplicity. Results are displayed at $p < 0.05$ corrected for multiple comparisons using 500 permutations (Winkler et al., 2014).

2.12. Statistical analysis

All statistical analyses for RNA-seq data are provided in the RNA and protein extraction with TRIzol, library construction, sequencing and analysis section. For all other tests, data were analyzed using GraphPad Prism software. *p*-Values for all pairwise comparisons were determined using unpaired (two-sample) *t*-tests. For comparisons between multiple groups, one-way multifactorial analysis of variance followed by Tukey post hoc tests were performed. *p*-Values are provided as stated by GraphPad Prism software, and significance was determined with *p*-values less than 0.05. Standard error of the mean was used in all graphs. For all quantification with statistical analysis, samples size is provided in the figure legends (n = biological replicate and refers to number of mice/samples used in each experiment).

3. Results

3.1. Gene profiling predicts a western diet causes vascular and myelin perturbations

High-fat diet, WD, and obesity have been shown to induce cognitive decline in both humans and mice (Elias et al., 2005; Kanoski and Davidson, 2011; Pistell et al., 2010; Valladolid-Acebes et al., 2011) but the mechanisms are not well understood. To address this, the impact of chronic consumption of a WD on the brains of male C57BL/6J (B6) mice was assessed (Fig. S1). The WD was developed previously to mimic diets commonly consumed in the western world (Graham et al., 2016). To avoid confounding effects of age-dependent estrogen changes (see Methods), only male mice were used in this study. Mice were fed a WD from 2 to 12 months. In B6 mice, 12 months is commonly considered middle-aged (Flurkey et al., 2007) and so our studies model midlife obesity in human populations. For the purpose of this study, herein after, we refer to 3.5 months as "young" and 12 months as "aged." Control B6 mice were fed a standard control chow diet (see Methods, Fig. S1). Significant weight increases were seen in WD-fed mice at 12 months (Fig. S1), despite no significant difference in food intake comparing control and WD-fed mice (Fig. S1). In addition, a significant decline in forepaw grip strength (force) was observed in aged WD-fed mice compared to young chow-fed and young WD-fed mice (Fig. S1).

To determine the genes and pathways that were altered as a result of the WD, transcriptional profiling was performed on brain samples from young and aged WD-fed and chow-fed mice. Two brain regions were profiled: (i) the HP and (ii) the FPC/CC (Fig. 1A and E). In total, 32 samples were separately profiled—2 brain regions from 4 mice from 2 age groups fed 2 diets. Pairwise analyses comparing young chow samples to both aged chow and WD samples were performed to determine DE genes (see Methods).

First, to identify the diet-specific effects (independent of aging), the aged control chow and aged WD samples were compared. A total of 411 genes were DE in the HP (Fig. 1B) and 1238 genes were DE in the FPC/CC. (Fig. 1F). Enrichment of Gene Ontology (GO) terms was determined using The Database for Annotation, Visualization and Integrated Discovery (DAVID v 6.7). GO terms are a set of controlled vocabulary to assign Biological Processes, Molecular Functions, and Cellular Components to genes based on experimental evidence or computational predictions. GO term analysis of the 411 DE genes in the HP showed an enrichment of genes relating to neuronal function (neuron differentiation, neuron migration, and synaptic transmission), axon guidance, and vascular control (regulation of blood pressure, regulation of angiogenesis, regulation of heart rate) (Fig. 1C). These data suggested the WD caused perturbations to both neuronal health and to support cells including glial cells and cells that form the cerebrovasculature (e.g., endothelial cells, astrocytes, pericytes). Many of the downregulated DE genes were associated with regulation of blood pressure and angiogenesis suggesting a reduction in the health of the cerebrovasculature. GO term analysis of the 1238 DE genes in the FPC/CC showed an enrichment of genes involved in ion/cellular homeostasis, immune responses, myelination (nerve impulse, axon ensheathment, axon potential in neurons, myelination of CNS), and gliogenesis (Fig. 1G). These GO terms suggested the WD altered inflammatory processes and axonal health/maintenance. Specifically, the axon/myelin-related terms suggested oligodendrocyte function may be affected by a WD.

Next, to identify the age by diet effects, the young control chow and aged WD samples were compared. A total of 335 genes were DE in the HP (Fig. 1B) and 381 genes were DE in the FPC/CC (Fig. 1F). GO term analyses of the 335 DE genes in the HP using DAVID identified enrichment of cell proliferation, vascular control (e.g., blood circulation and blood vessel development), and immune response (Fig. 1D). Terms relating to vascular control and immune responses were also enriched in the aged control chow versus WD comparison (Fig. 1C). However, the enrichment of GO terms such as acute immune responses, acute inflammatory response, and classical complement cascade in this age by diet comparison suggested a synergistic relationship between age and WD consumption with respect to inflammatory responses. GO term analyses of the 381 DE genes in the FPC/CC showed enrichment of terms including immune response, axonogenesis, and inflammatory response (Fig. 1H). This analysis again pointed toward the WD impacting

axon/myelin health/maintenance and neuroinflammation (particularly innate immune response such as complement activation)—processes that are potentially influenced by an age-dependent consumption of the WD (i.e., an age by WD affect).

From the GO term analyses described previously, we were most intrigued by the myelination- and inflammation-related terms enriched in the 1238 DE genes in the FPC/CC comparing aged control chow to aged WD samples (Fig. 1F–H). To further investigate these findings, we used GOrilla that allowed us to visualize Molecular Function and Cellular Component GO terms (Fig. 1I–J). Providing further evidence of myelin changes, GOrilla showed that the most enriched Molecular Function term in the 1238 DE genes was dysfunction in the structure of myelin sheath (Fig. 1I). Interestingly, the analysis of Cellular Component terms (Fig. 1J) identified the term connexin complex as enriched. Three connexins (*Gjb1*, *Gjb2*, and *Gjc2*) are DE in the FPC/CC in the aged

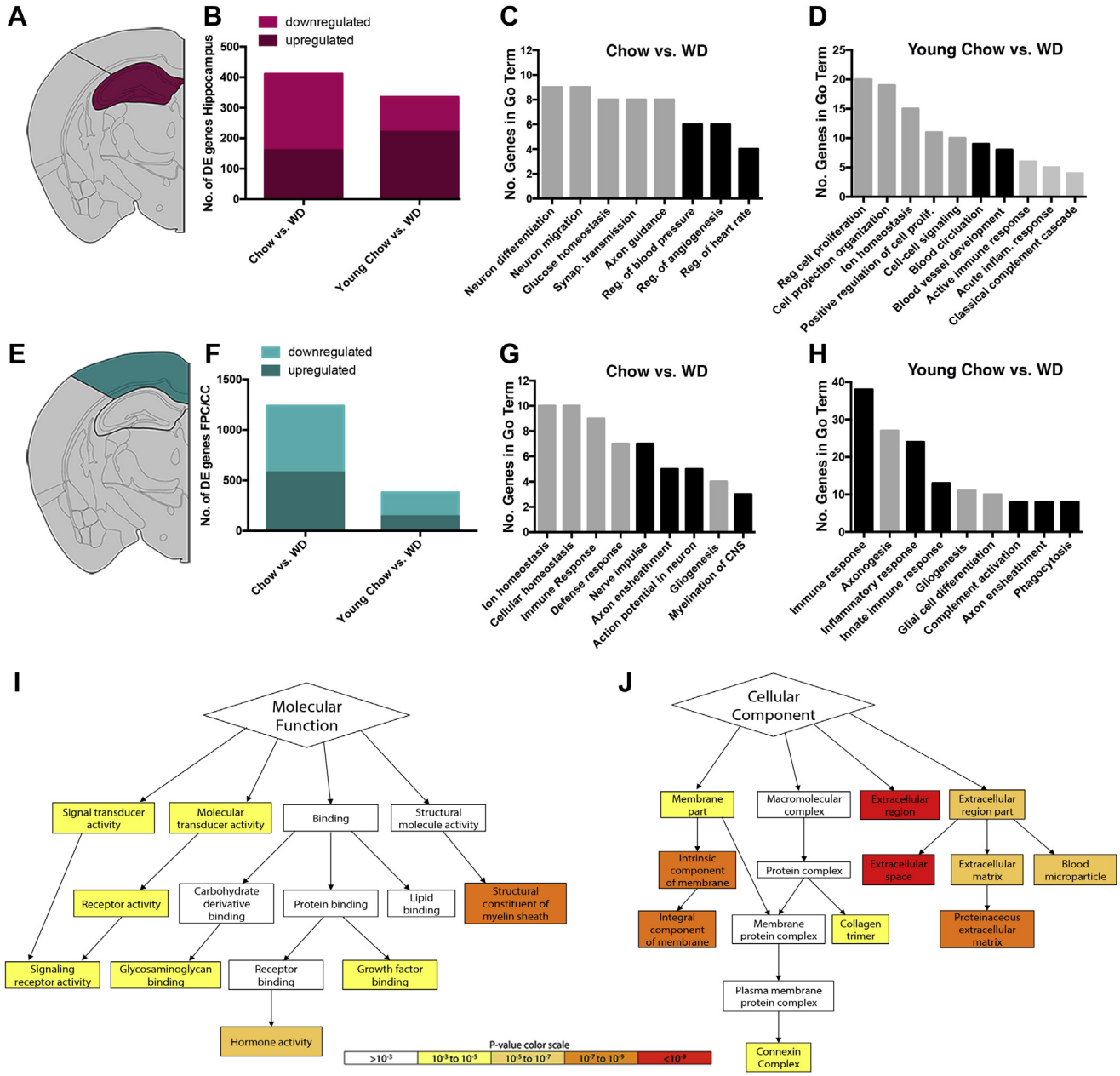

Fig. 1. Transcriptional profiling predicts WD affects myelin integrity, cerebrovasculature, and immune responses. (A) Depiction of the hippocampus (HP) that was dissected for RNA sequencing. (B) The number of differentially expressed (DE) genes in the HP comparing aged WD with aged chow mice (left) and aged WD with young chow-fed mice (right). (C) GO terms overrepresented in the DE genes in the HP comparing aged WD with aged chow mice. Black bars represent GO terms associated with cerebrovascular health. (D) GO terms overrepresented in the DE genes in the HP comparing aged WD with young chow (all bars). Black bars represent terms involved in cerebrovascular health (E) Depiction of the frontoparietal cortex and corpus callosum (FPC/CC) that was dissected for RNA sequencing. (F) The number of DE genes in the FPC/CC comparing aged WD with aged chow mice (left) and aged WD with young chow-fed mice (right). (G) GO terms overrepresented in the DE genes in the FPC/CC comparing aged WD with aged chow (all bars). Black bars represent GO terms associated with myelination/oligodendrocyte function. (H) GO terms overrepresented in the DE genes in the FPC/CC comparing aged WD with young chow (all bars). Black bars represent GO terms associated with myelination/oligodendrocyte function and myeloid cell function. (I) A subset of Molecular Function GO terms overrepresented in the DE genes comparing aged WD with aged chow mice in the FPC/CC highlighting the significance of myelin sheath–related genes. (J) A subset of Cellular Component GO terms overrepresented in the DE genes comparing aged WD with aged chow mice in the FPC/CC highlighting the significance of extracellular matrix–related genes. Data for I and J were predicted using GOrilla, an online tool to visualize GO terms.

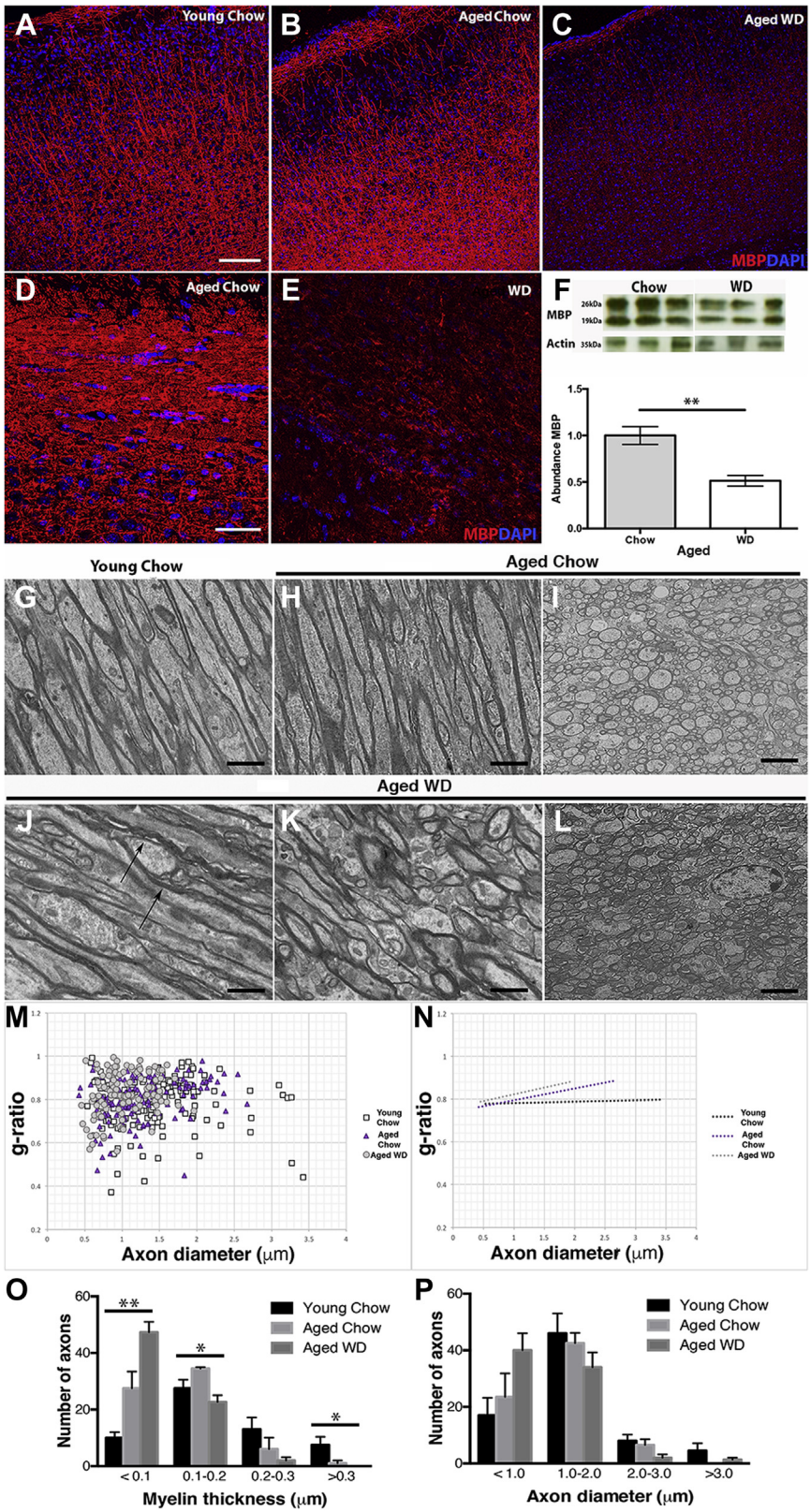

Fig. 2. Myelin integrity is compromised in WD mice. (A–E) By immunofluorescence, aged WD mice show decreased myelin basic protein (MBP, red) within the FPC (A–C) and corpus callosum (D–E) compared to young and aged chow mice. (F) The reduction in MBP was confirmed by western blotting ($p = 0.0014$). (G–L) Electron microscopy (EM) in both coronal (G, H, J, K) and sagittal (I, L) brain sections confirmed myelin damage in aged WD fed mice. Young and aged chow mice showed densely packed myelin sheaths surrounding the axons of the corpus callosum (G–I), whereas aged WD mice showed loosely packed myelin sheath surround axons with areas of ballooned myelin (arrows, J–L). (M) Scatter plot graphs display g-ratio (y-axis) in relation to axon diameter (x-axis) of individual axon fibers. At least 200 myelinated axons were considered for each group. (N) The linear regression of the g-ratio measurements for each condition (at least 130 myelinated axons, n = 4). (O) Distribution plots for myelinated thickness for axons of young chow, aged chow, and aged WD. There are significantly more axons with myelin that is <0.1 μm in samples from aged WD mice compared to both young chow and aged chow mice (**ANOVA $p = 0.0036$,

WD versus control chow comparison. Connexins are gap junctions that form cell-to-cell channels that facilitate the transfer of ions and small molecules (Orthmann-Murphy et al., 2008). *Gjb1*, *Gjb2*, and *Gjc2* are expressed by oligodendrocytes and astrocytes (Ahn et al., 2008; Sargiannidou et al., 2009; Wasseff and Scherer, 2011) suggesting a dysregulation in the connections involving astrocytes and oligodendrocytes. The most enriched terms in the Cellular Component analyses related to extracellular region, extracellular matrix, and proteinaceous extracellular matrix (Fig. 1J). Although vascular-related GO terms were not enriched in the previous analyses using DAVID (Fig. 1F–H), this finding using GOrilla predicts WD modified basement membrane proteins (such as collagens and laminins) that surround the cerebrovascular in the FPC/CC.

3.2. A western diet causes myelin loss and structural abnormalities of the white matter

Transcriptional profiling of the FPC/CC predicted structural changes to myelin and oligodendrocyte activity in WD-fed mice (Fig. 1). To validate these findings, a detailed characterization of myelin integrity was performed. A significant reduction in MBP, a major constituent of the myelin sheath (Ainger et al., 1997; Sternberger et al., 1978), was observed by immunofluorescence comparing brain sections from both the FPC and CC of WD-fed to chow-fed mice (Fig. 2A–E). To quantify MPB protein levels, western blotting was performed. There was a 50% reduction in MBP protein levels in the brains of aged WD-fed compared to aged chow-fed mice (Fig. 2F and Figs. S2). Furthermore, ultrastructural analyses using transmission electron microscopy showed normal densely packed myelin sheaths surrounding axons in the CC in both sagittal (Fig. 2G, H, J and K) and coronal (Fig. 2I and L) sliced brains of young and aged chow-fed mice compared to abnormal, loosely packed, ballooned myelin surrounding axons in aged WD-fed mice (Fig. 2J–L). Ballooned myelin has been shown previously in aged brains of rodents and primates and associated with type II diabetes and neuroinflammation (Mizisin et al., 2007).

To quantify myelin integrity, g-ratios (myelin thickness compared to axon diameter) (Chomiak and Hu, 2009; Rushton, 1951) were calculated. The g-ratios of aged WD-fed and aged chow-fed mice were compared to young chow-fed mice. There was an observable difference in g-ratios comparing aged WD-fed mice to either aged chow or young chow mice (Fig. 2M–P). Specifically, there was a significant increase in the number of axons with myelin thickness less than 0.1 μm in aged WD-fed mice compared to both young and aged chow-fed mice (Fig. 2O). Although trending, there was no significant difference between aged chow-fed and young chow-fed mice. There was also a significant decrease in axons with myelin thickness of 0.1–0.2 μm and >0.3 μm in aged WD-fed mice compared to young and aged chow-fed mice (Fig. 2O). However, there were significant differences in axon diameter comparing aged WD-fed mice to young or aged chow-fed mice (Fig. 2P). Together, these data are consistent with the WD causing myelin thinning.

3.3. A western diet causes cerebrovascular damage

Previous studies, including our own, have shown cerebrovascular decline occurs with age in both humans and mice (Bell et al., 2010; Iturria-Medina et al., 2016; Montagne et al., 2015; Soto et al., 2015). In this study, transcriptional profiling predicted the WD caused cerebrovascular changes in the HP and FPC/CC (Fig. 1). To validate these predictions, key components of the neurovascular unit (NVU) including endothelial cells, astrocytes, pericytes, and vessel-associated basement membrane protein laminin were assessed by immunofluorescence and confocal microscopy. All images were standardized to chow-fed controls (see Methods). Cell number quantification was performed by manual counting of 20× images, fluorescence area was determined using a FIJI plugin (see Methods). At least 4 images from at least 4 samples per group were assessed.

There was a significant decrease in CD31+ density comparing aged WD mice to either young WD mice or young chow mice (Fig. 3A–C). However, there were no significant differences in endothelial cell density comparing aged WD mice to aged chow mice or aged chow with young chow-fed mice. These data suggest that endothelial cell density is affected by an interaction between aging and WD (i.e., chronic consumption) and not simply by either aging on a chow diet or short-term WD exposure. In contrast to endothelial cell density, there was a significant increase in GFAP+ reactive astrocytes in aged WD compared to aged chow mice (Fig. 3A, B and D). Astrocyte reactivity was not quantified for young chow or young WD mice as there were insufficient numbers of GFAP+ cells in the cortex to produce meaningful results. There were 30% fewer PDGFRβ+ pericytes in the cortex of aged WD compared to aged and young chow mice (Fig. 3E–H). Finally, there were both age-dependent and diet-dependent decreases in laminin area and evidence of extravascular fibrin deposits in the cortex of WD mice compared to chow mice (Fig. 3I–M).

3.4. Cerebrovascular dysfunction precedes myelin loss in young western diet–fed mice

We would predict that WD would first induce cerebrovascular dysfunction and myeloid cell activation, which subsequently causes white matter damage and cognitive decline. To test this, 2-month B6 male mice were fed a WD for 6 weeks. Mice fed the WD for this short time gained a significant amount of weight compared to chow-fed controls (Fig. S3A). However, there was no evidence of cognitive deficits in these mice (Fig. S3B–E). We next assessed cerebrovascular, astrocyte, myeloid cell, and myelin changes in young WD-fed mice. There was a significant increase in astrocytes in the corpus callosum (Fig. S3F–H) that was accompanied by a decrease in laminin (Fig. S3I–K). In addition, young WD-fed mice had significantly more IBA1+ myeloid cells in FPC/CC and HP compared to young chow-fed mice (Fig. S4A–F). Importantly, no significant changes to the myelin or the number of OLIG2+ oligodendrocytes were observed in the corpus callosum (Fig. S4G–I). Therefore, cerebrovascular damage and increased myeloid cell numbers precedes myelin loss.

3.5. Obesity is associated with white matter integrity loss in older adults

To further support our findings in mice and previous human studies that had suggested white matter damage as a feature of obesity (Kullmann et al., 2016; Stanek et al., 2011), DTI data generated as part of the Alzheimer's disease Neuroimaging Initiative (ADNI) (Weiner et al., 2012) was assessed. DTI allows for the study of the microstructural properties of the brain that includes white matter tracts. Data were controlled for age, gender, diagnosis, and history of hyperlipidemia, hypertension, or diabetes by

F = 2.557 [DFn = 2, DFd = 7]). Conversely, there is significantly fewer axons with myelin that is 0.1–0.2 μm and >0.3 μm in aged WD mice compared to aged chow fed mice (*ANOVA $p = 0.0208$, F = 1.983 [DFn = 2, DFd = 8] and *ANOVA $p = 0.049$, F = 1.495 [DFn = 2, DFd = 8], respectively). (P) Distribution plots of axon diameter for myelinated axons of young chow, aged chow, and aged WD. There are no significant differences in axon diameter comparing samples from young chow, aged chow, and aged WD mice. Scale bars: A–C, 100 μm; D–E, 40 μm; G, H, J, K, 4 μm; I, L, 2 μm.

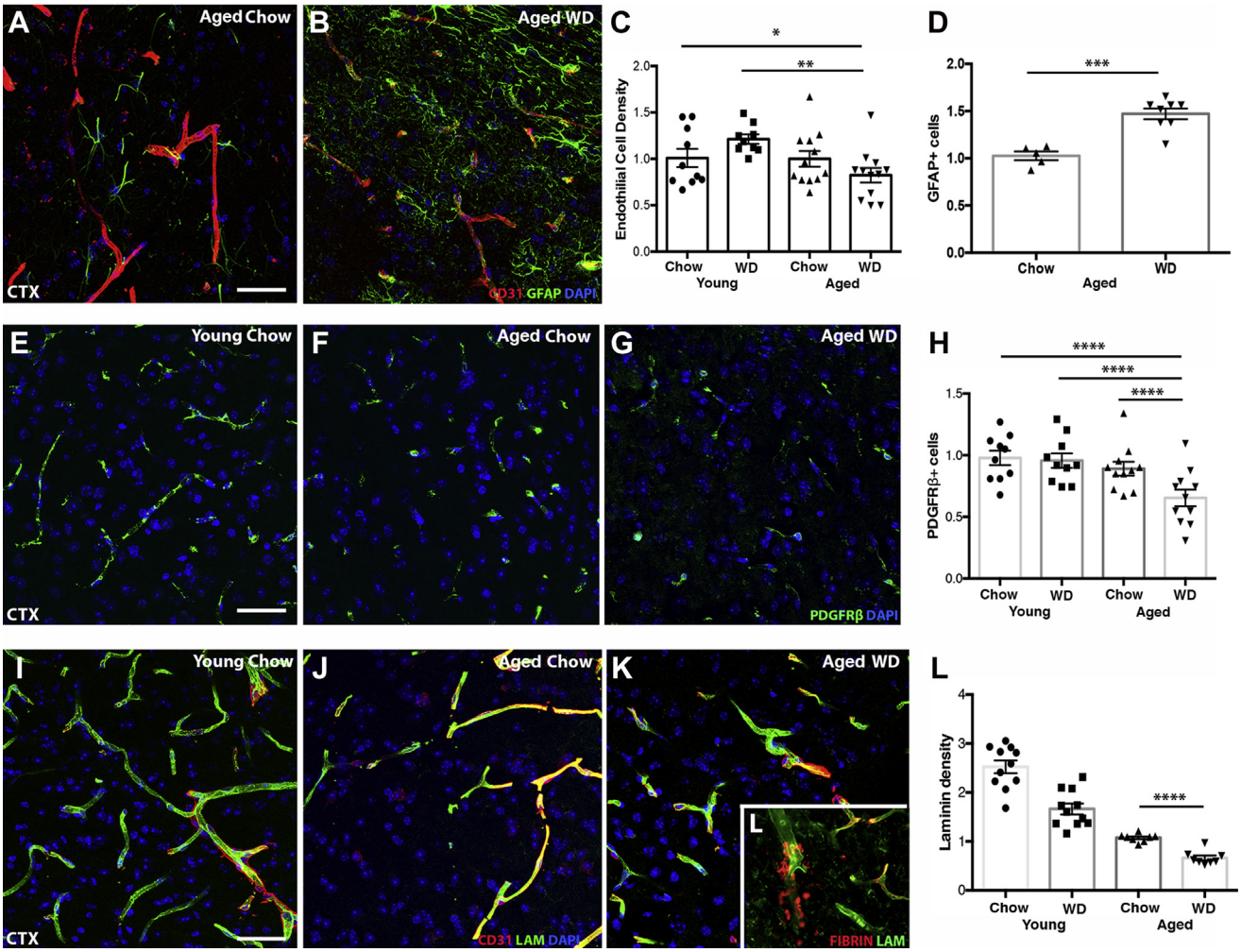

Fig. 3. WD induces cerebrovascular dysfunction and astrocyte reactivity. (A–C) Aged WD mice showed a significant reduction in CD31 (an endothelial cell marker) compared to young chow and young WD mice ($n \geq 11$, $^{*}p < 0.05$, $^{**}p < 0.01$). (D) Aged WD mice showed a significant increase in GFAP+ astrocytes compared to aged chow mice ($n \geq 5$, $^{***}p < 0.001$). (E–H) Aged WD mice showed significantly fewer pericytes (PDGFRβ) in the cortex compared to aged chow, young chow, and young WD mice ($n \geq 11$, $^{****}p < 0.0001$). (I–L) Aged WD mice showed significantly less laminin (LAM) compared to aged chow mice ($n \geq 8$, $^{****}p < 0.0001$). (L, inset) Representative image of a region showing fibrin deposited outside the vessels in aged WD mice. Scale bars for all images: 40 μm.

including these as covariates. Although multiple white matter tracts have been suggested to be affected by obesity (Bolzenius et al., 2015; Papageorgiou et al., 2017), we focused on the corpus callosum as this was the region assessed in our mouse studies. Obese individuals (defined as a BMI $\geq$ 30; n = 54) showed significantly reduced FA, a nonspecific measure of white matter integrity, in widespread white matter regions relative to nonobese individuals (defined as a BMI < 30; n = 202; Fig. 4A and B), including the corpus callosum and anterior corona radiata. When evaluated on a regional basis, the high BMI group mean FA was significantly reduced in the corpus callosum in the full sample and in CN older adults only (Fig. 4B; $p < 0.05$). Furthermore, MD, a measure of decreased axonal membrane density, edema, and degeneration was significantly increased in the right frontal lobe of obese individuals relative to nonobese individuals (Fig. 4C and D). On regional analysis of the corpus callosum, significant differences were observed in the CN-only group, where obese individuals showed higher MD in the corpus callosum than nonobese individuals (Fig. 4D, $p < 0.05$). Finally, RD, a measure of demyelination, was significantly increased in obese individuals relative to nonobese individuals in widespread regions, including throughout the corpus callosum and frontal white matter (Fig. 4E and F). On regional analysis of the corpus callosum, RD was significantly higher in the obese individuals, relative to the nonobese individuals in the CN-only analysis (Fig.4F, $p < 0.05$). No differences in AD were observed in either the full sample or CN-only group. These findings were independent of age, gender, diagnostic group (CN, MCI, Alzheimer's disease), and history of comorbidities (such as hypertension, hyperlipidemia, and diabetes).

3.6. WD-fed mice show increased numbers of oligodendrocytes in white matter tracts

Despite an overall reduction in MBP protein levels, disorganization of myelin and decreased g-ratios in the FPC/CC of aged WD compared to chow mice (Fig. 2), transcriptional profiling indicated myelin-related genes were upregulated (Fig. 1). These include *Mbp* (1.699), *Otf2* (1.48), *Plp* (1.26), *Mog* (1.30), *Mobp* (1.58), *Mag* (1.52), and *Myrf* (1.51) (Fig. 5A). Furthermore, using a riboprobe for the proteolipoprotein (*Plp*) gene (expressed in mature, myelin producing oligodendrocytes (Cai et al., 2010; Fumagalli et al., 2011)), a greater number of *Plp*-expressing oligodendrocytes were observed in the HP, FPC, and CC of aged WD-fed compared to aged chow-fed mice (Fig. 5B–C). To quantify the numbers of oligodendrocytes and

oligodendrocyte precursors, immunofluorescence using antibodies against OLIG2 (all oligodendrocytes and precursors) and CC1 (mature oligodendrocytes) was performed. There was a significant increase in both the numbers of OLIG2+ cells (Fig. 5D–I and L) and CC1+ cells (Fig. 5H–K and M) in the corpus callosum of aged WD-fed compared to chow-fed mice. In WD-fed mice, there were many more OLIG2+ cells (average = 99.8 cells/20× image) compared to CC1+ cells (average of 19.5 cells/20× image) suggesting a significant proportion of the OLIG2+ cells were immature oligodendrocytes.

3.7. WD-fed mice show increases in CD8+IBA1+ myeloid cells

Gene profiling of the FPC/CC and the HP showed an increase in myeloid cell genes *Trem2* (1.68), *Tyrobp* (2.36), and the phagosome marker *Cd68* (1.68) in aged WD-fed compared to chow-fed mice (Figs. 1 and 5A). To further characterize myeloid cells, IBA1+ cells were assessed in the corpus callosum. As expected, given the increase in IBA1+ cells in the short-term diet study (Fig. S4), there was a significant increase in IBA1+ cells within the corpus callosum of aged WD-fed compared to aged chow-fed mice (Fig. 6A–C). Unlike chow-fed mice, most IBA1+ cells in the WD-fed mice also expressed CD68, a commonly used marker of activated or phagocytic cells (Fig. 6A–B). Next, using three-dimensional reconstructions of the confocal images using IMARIS software (see Methods), MBP was localized next to and within IBA1 regions (Fig. 6D–G). This close proximity of CD68+IBA1+ cells to myelin tracts suggests the white matter damage may be a result of phagocytosis of myelin by myeloid cells.

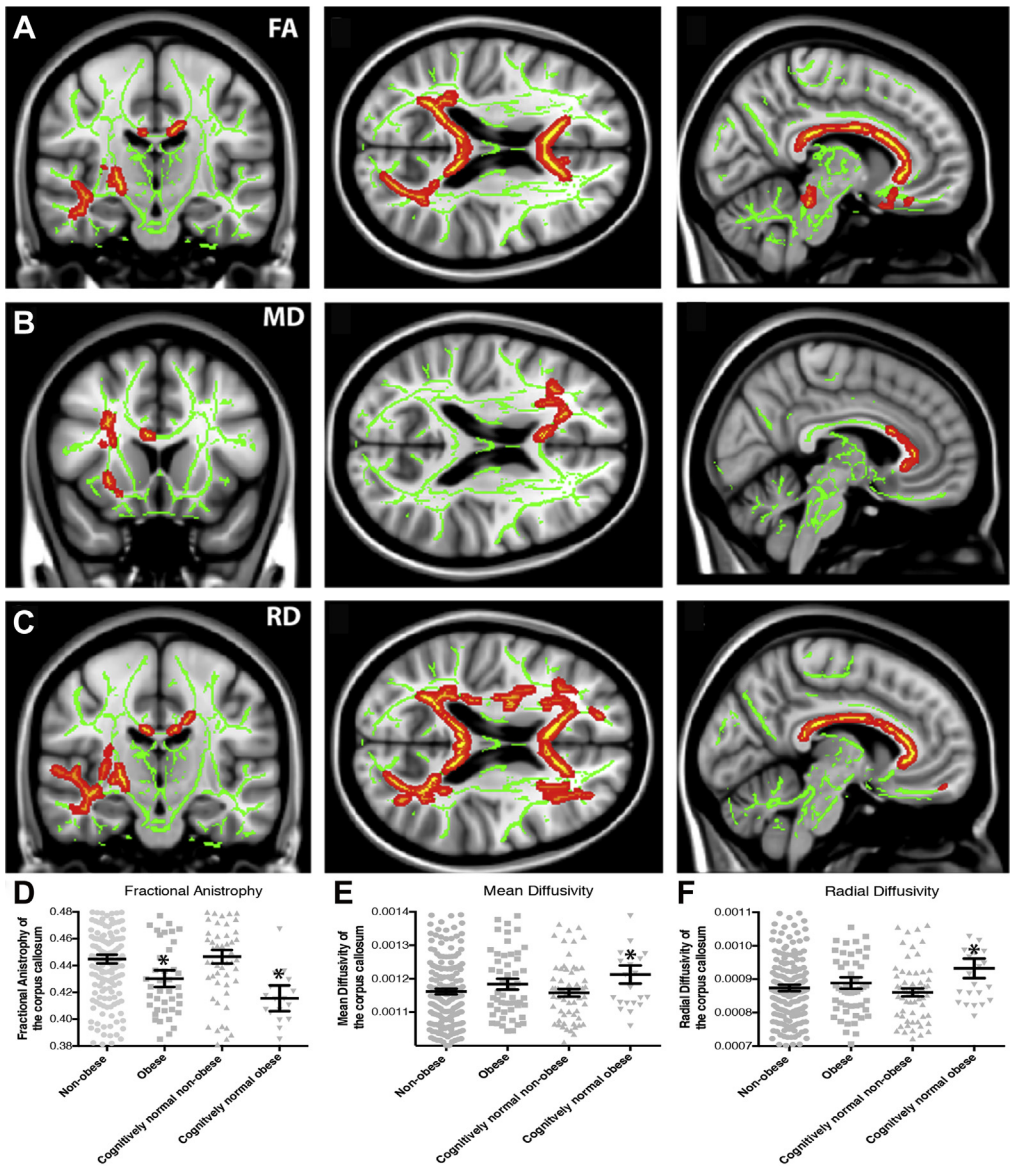

Fig. 4. White matter integrity is decreased in obese individuals. Cognitively normal older adults (CN) and patients with mild cognitive impairment (MCI) and Alzheimer's disease (AD) who are obese (BMI ≥ 30) showed reduced white matter integrity relative to nonobese (BMI < 30) individuals. (A and B) Reductions in fractional anisotropy (FA), a general measure of white matter integrity, were observed in obese (n = 54) relative to nonobese (n = 202) individuals throughout the corpus callosum and frontal white matter. (B) On a regional basis, mean FA in the corpus callosum was reduced in obese relative to nonobese individuals both in the full sample and in CN older adults only (n = 88, $^*p < 0.05$). (C and D) Increased mean diffusivity (MD), a reflection of increased white matter damage, was also observed in the frontal white matter in obese relative to nonobese individuals. (D) Regional analysis shows a significant increase in MD in the corpus callosum only in CN individuals ($^*p < 0.05$). (E and F) Increased radial diffusivity (RD), reflecting either demyelination or axonal swelling, was also observed in obese relative to nonobese individuals in the corpus callosum and frontal white matter. (F) Upon regional analysis, mean corpus callosum RD was increased in obese relative to nonobese individuals in the CN-only group ($^*p < 0.05$).

3.8. Exercise prevents western diet–induced cognitive deficits, white matter damage, and cerebrovascular decline

Increased physical activity, such as running, has been shown to have beneficial effects to multiple diet- and obesity-related outcomes and comorbidities (Lavie et al., 2015; Ruegsegger et al., 2015; Williams and Thompson, 2013), including frailty, anxiety and cognitive decline. (Dishman et al., 2006; Lavie and Milani, 2004; Villareal et al., 2006). However, the impact of running on white matter damage has never been tested. Therefore, mice were provided running wheels at 1 month and WD at 2 months (Fig. 1). Appropriate sedentary and control chow-fed mice were also included. Although there was a significant reduction in weight between running and sedentary WD-fed mice, running WD-fed mice still showed a significant increase in weight compared to either sedentary or running chow-fed mice (Fig. 7A). This was independent of the distance run by either of the

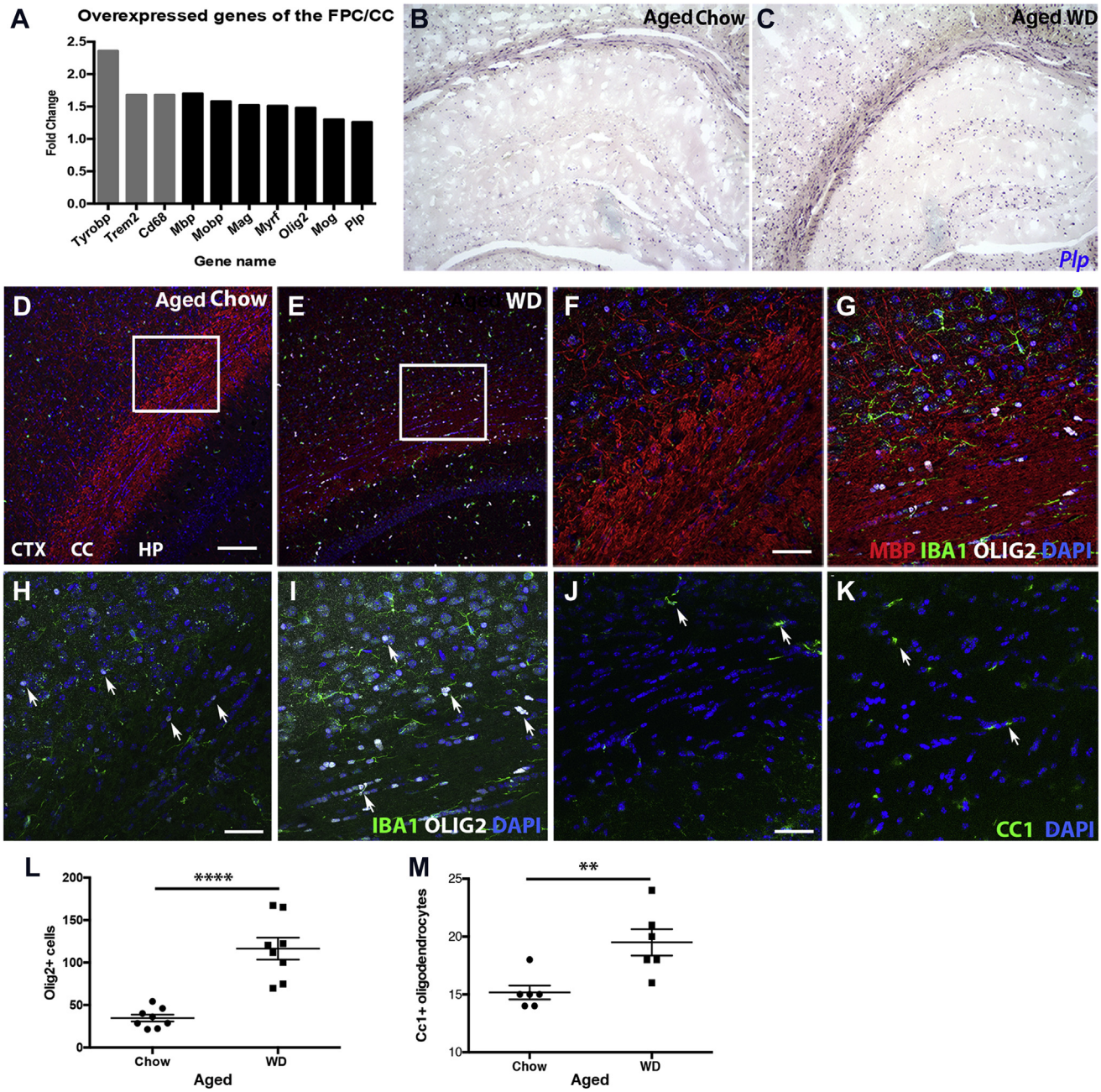

Fig. 5. WD-induced white matter damage is caused by unbalanced myelin turnover. (A) Gene expression analysis of the FPC/CC showed genes associated with phagocytosis (gray bars), myelin maintenance, and oligodendrocytes (black bars) were upregulated in aged WD compared to aged chow mice. (B and C) By RNA in situ hybridization, expression of *Plp*, a marker of mature oligodendrocytes, was greater in the cortex, corpus callosum, and hippocampus of aged WD compared to aged chow mice. (D and E) By immunofluorescence, aged WD mice showed a significant increase in OLIG2+ oligodendrocytes in both the FPC and corpus callosum. (F and G) Higher resolution images of the areas from the inlays in E and F showed OLIG2+ cells aligned in the corpus callosum of aged WD mice. (H and I) Higher resolution images of the areas from the inlays in E and F without myelin staining showed OLIG2+ cells aligned in the corpus callosum of aged WD mice (arrows, OLIG2+ cells, white). (J and K) By immunofluorescence, aged WD mice showed a significant increase in CC1+ oligodendrocytes in the corpus callosum (arrows, CC1+ cells, green). (L) OLIG2+ cells are significantly increased in the corpus callosum in aged WD compared to aged chow mice ($n = 8$, $^{****}p < 0.0001$). (M) CC1+ cells are significantly increased in the corpus callosum in aged WD compared to aged chow mice ($n = 6$, $^{**}p < 0.01$). Scale bars: D–E, 100 μm; F–K, 40 μm.

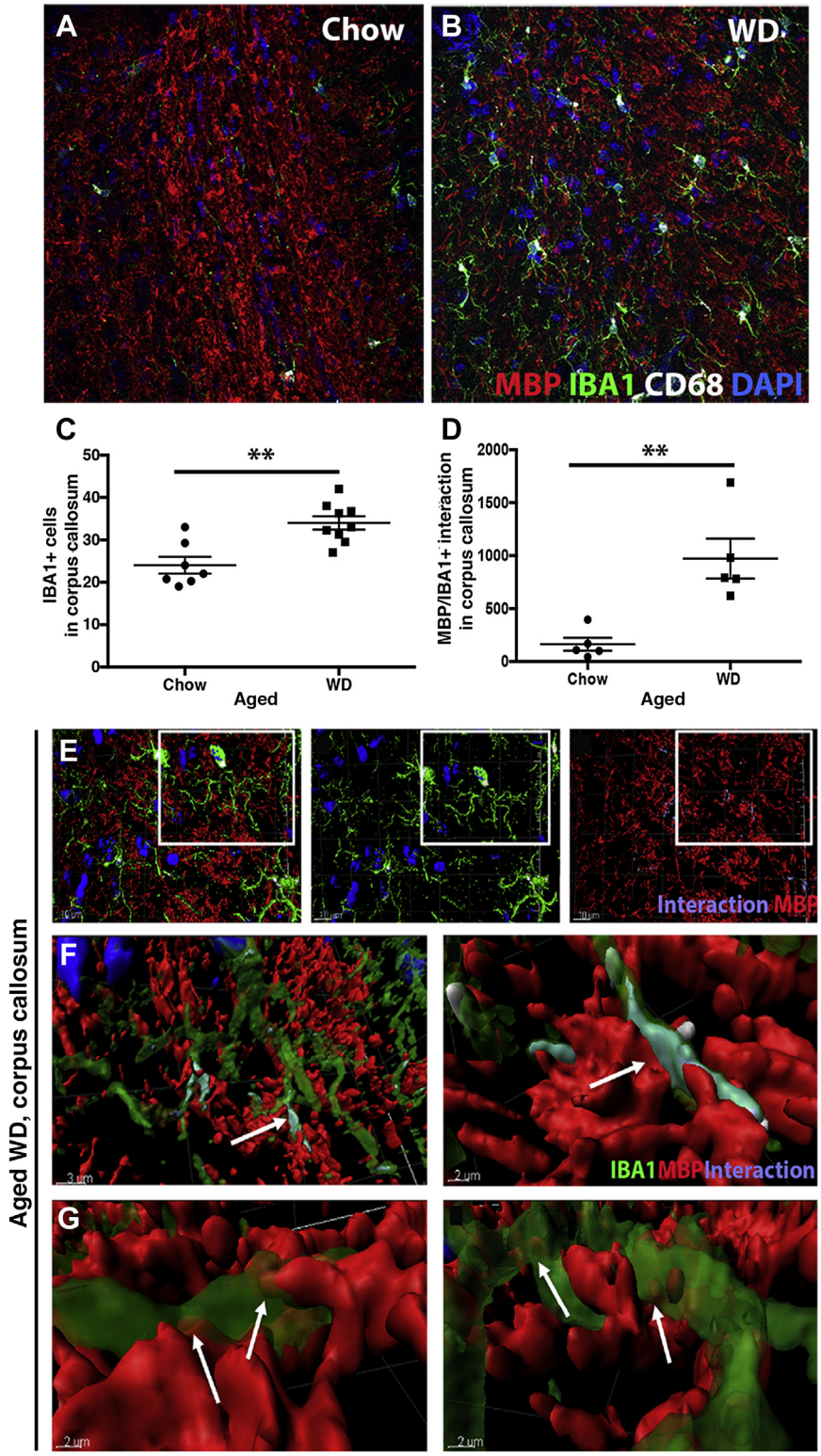

Fig. 6. WD causes activation of phagocytosing myeloid cells. (A and B) A representative image of the corpus callosum from an aged WD mouse showing myelin (MBP), myeloid cells (IBA1), and phagosome-containing myeloid cells (CD68). (C) There was a significant increase of IBA1+ cells in the corpus callosum of aged WD compared to aged chow mice ($n \geq 7$, $^{**}p = 0.0012$). (D) Myelin-myeloid cell interactions were also significantly increased in aged WD compared to aged chow mice ($n \geq 5$, $^{**}p = 0.0035$). (E–G) IMARIS was used to identify myeloid cells that were actively phagocytosing myelin. The image shows activated myeloid cells interacting with myelin visualized with anti-MBP (E). F and G are higher resolution images from the boxed region in E and show MBP (red) contacting myeloid cells (green). Labeling in purple shows the interactions between CD68+IBA1+ cells. Arrows (F and G) show MBP inside the cell body of the myeloid cells.

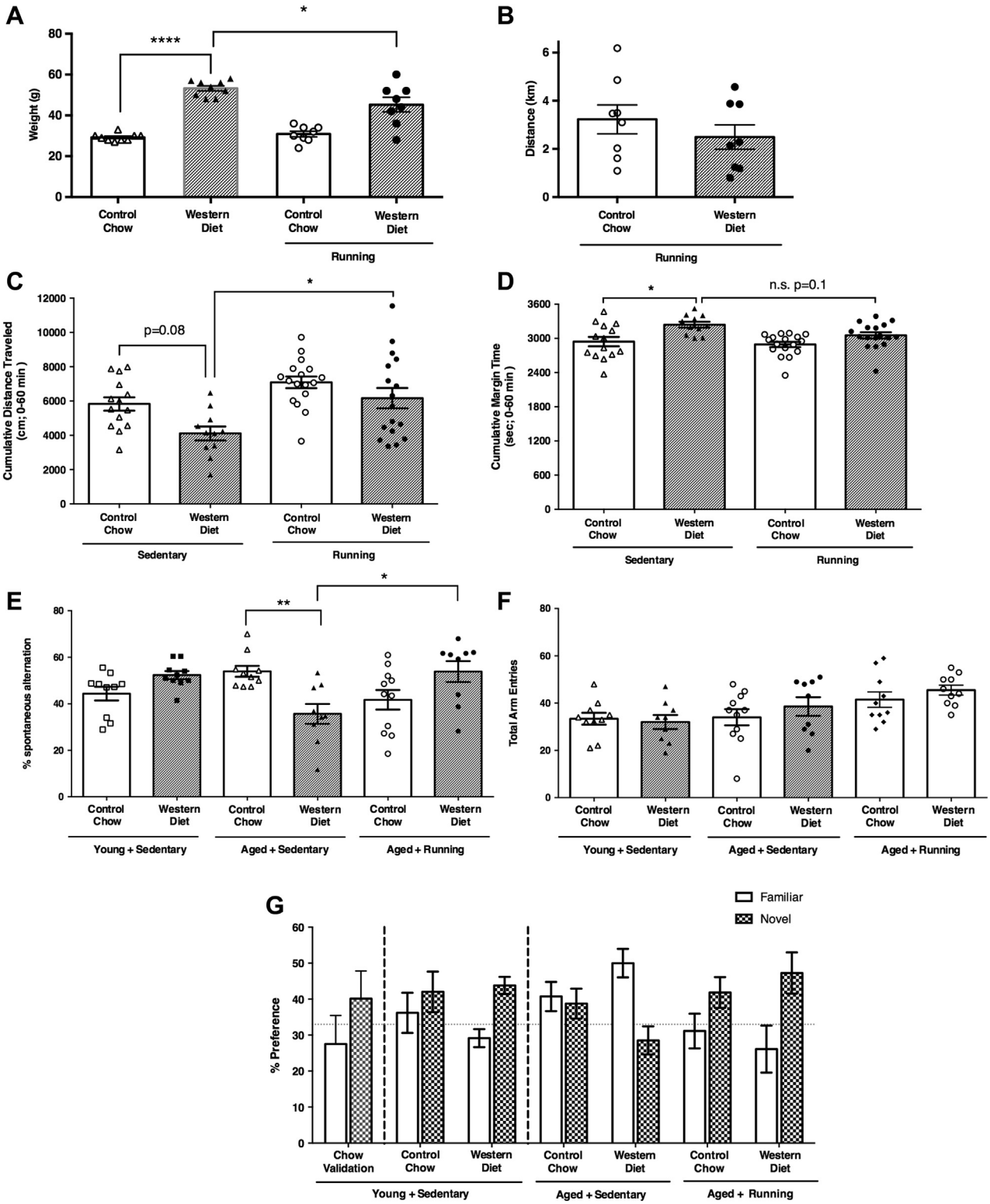

Fig. 7. Running prevents age- and WD-induced cognitive deficits. (A) Aged WD mice, irrespective of sedentary or running, demonstrated significant increases in body weights related to aged state-matched controls (n ≥ 8, sedentary chow vs. sedentary WD $^{****}p < 0.0001$, sedentary WD vs. running WD $^{*}p < 0.03$). (B) Aged WD mice demonstrated wheel running activity levels comparable to that of aged running chow mice with no significant differences between groups (n = 8, $p = 0.375$). (C) Activity levels in the open field as measured by cumulative distance traveled revealed a significant reduction in aged sedentary WD mice relative to aged sedentary chow subjects. Activity levels were significantly increased in aged running WD compared to aged sedentary WD mice. (D) Aged sedentary WD mice demonstrated significant increases in time spent at the margin of the open field, relative to aged sedentary chow mice, indicative of an anxiogenic-like phenotype. Running produced a modest, nonsignificant attenuation in cumulative margin time comparing aged running WD with aged sedentary WD mice ($p = 0.1$). (E–F) Young sedentary WD mice and young sedentary chow mice showed no significant impairment in % correct alternations. However, aged sedentary WD mice showed a significant impairment in % correct alternation (E, n = 9 $^{**}p < 0.001$, $^{*}p < 0.5$), which was not due to reductions in total activity as measured by total arm entries (F). Running significantly improved the WD induced deficit in % alternation in aged mice. (G) Short-term memory was intact in young sedentary mice regardless of diet as indicated by a preference for novel versus familiar in a novel spatial recognition task. Aged sedentary mice failed to demonstrate a preference for the novel arm indicative of impaired short-term memory while running prevented/protected short-term memory as both aged chow and WD mice with access to a running wheel demonstrated the expected preference for the novel versus familiar arm.

groups (Fig. 7B) suggesting the benefits of exercise on the aging brain of obese mice are not solely due to weight loss.

First, to determine the effects of WD with and without voluntary running on cognitive ability and related behaviors, WD-fed and chow-fed mice were assessed through a battery of behavioral tests (Fig. 7C–G). Open field activity in WD mice in the absence of a running wheel revealed significant reductions in exploration time as measured by cumulative distance traveled over a 60-minute period, relative to sedentary mice on control chow. In the presence of a running wheel, exploratory activity levels were restored in WD mice relative to sedentary WD mice and interestingly to a level of activity demonstrated in chow-fed mice (Fig. 7C). Thigmotaxis behavior in the open field, as measured by time spent at the margin of the arena and indicative of an anxiogenic-like phenotype, was significantly increased in sedentary WD mice relative to sedentary chow mice (Fig. 7D). Access to a running wheel did not significantly reduce thigmotaxis behavior although there was a modest reduction in running WD mice relative to sedentary WD mice ($p = 0.1$) (Fig. 7D).

Hippocampal working memory as assessed in the spontaneous alternation task revealed no significant differences in young mice irrespective of diet (Fig. 7E). In aged mice, however, WD consumption resulted in a significant reduction in % alternations indicative of impaired spatial working memory, relative to age-matched chow mice. Spatial working memory was restored in aged WD mice with access to a running wheel (Fig. 7E). Importantly, there were no significant differences in motor activity as measured by total arm entries (Fig. 7F). In the novel spatial recognition task, intact short-term memory is indicated by a preference for spending a greater % of time in the novel arm versus the familiar arm. Young sedentary mice regardless of diet demonstrated the expected preference for the novel arm versus the familiar arm (Fig. 7G). However, sedentary aged mice (irrespective of diet) did not demonstrate a preference for the novel arm versus the familiar arm indicative of impaired short-term memory. Both running aged WD and running aged chow mice demonstrated intact short-term memory as measured by a preference for the novel versus the familiar arm of the maze (Fig. 7G).

Next, the effects of running on WD-induced cerebrovascular dysfunction, myelin loss, and myeloid cell numbers were assessed in the FPC/CC region. Running prevented WD-induced cerebrovascular changes including the reduction in endothelial cell and pericyte numbers (Fig. 8A–B) as well as the increase in reactive astrocytes (Fig. 8C). Running aged WD mice also showed significantly fewer microglia compared to young chow sedentary control and trended lower when compared to aged sedentary WD mice (Fig. 8D). IMARIS was then used to quantify the effects of running on WD-induced myelin loss and myeloid cell numbers (Fig. 8E–L). Although not significant, myelin levels were generally increased in running aged WD compared to sedentary aged WD mice (Fig. 8I). This may suggest some mouse-to-mouse variability in the effect of running on WD-induced white matter damage and may be as a result of individual differences in diet consumption or running distances. However, running prevented the increase in IBA1+ cells in the corpus callosum (Fig. 8J) and the levels of MBP-IBA1 interactions seen in sedentary WD-fed compared to chow-fed mice (Fig. 8K). There was a significant increase in CD68+ surfaces in WD-fed compared to chow-fed mice that was prevented by running (Fig. 8L). These data support the model that white matter damage in WD-fed mice may be due in part to the increase in numbers of CD68+IBA1+ phagocytosing myeloid cells.

4. Discussion

The long-term effects of a WD and sedentary lifestyle are of great interest to better understand the environmental risk factors for age-related cognitive decline, dementias, and other neurodegenerative diseases. It is known that diet, obesity, and physical inactivity can have direct effects on the structure and function of the brain (Gray et al., 2006; Medic et al., 2016; Tucsek et al., 2014; Veit et al., 2014) but the precise mechanisms have not previously been determined. To study this, we used a mouse model of WD-induced obesity to elucidate the damaging effects of WD-induced neuroinflammation and cerebrovascular damage on white matter in the FPC, corpus callosum, and HP. White matter density via magnetic resonance imaging has been correlated to cognitive function (Turken et al., 2008), suggesting that the white matter damage we observed may contribute to the cognitive decline. Structural changes to white matter have been associated with obesity and the aging brain (Feldman and Peters, 1998; Kullmann et al., 2015; Peters, 2009). We also further corroborated the importance of these findings to obesity in the human population. Based on DTI data from the ADNI cohorts (Petersen et al., 2010), high BMI ($\geq$30) correlated strongly with a general breakdown of white matter integrity and changes in radial diffusivity in the corpus callosum suggesting demyelination or axonal swelling. Previous studies correlated high BMI with lower gray matter volume and changes to white matter density in humans (Kalaria, 2010; Kullmann et al., 2015, 2016; Medic et al., 2016; Stanek et al., 2011; Veit et al., 2014), but this is the first time the ADNI cohort has been analyzed in this manner. In both the mouse and human studies, we chose to focus on the corpus callosum as this was the white matter tract that was profiled by RNA-seq in the mouse and showed the greatest differences in MBP protein levels assessed by immunofluorescence. However, obesity and high BMI have also been shown to affect other white matter tracts including the anterior and posterior thalamic radiation, the uncinate fasciculus, the internal capsule and the cingulum (Bolzenius et al., 2015; Papageorgiou et al., 2017). It is still to be determined whether the WD mice and the ADNI cohorts also show similar white matter changes in other brain regions.

Our data support a model in which white matter damage is due to changes in cells necessary for myelin turnover—a process that occurs throughout adulthood to prevent neuronal functional decline. The production of myelin by oligodendrocytes and the removal of myelin fragments by phagocytosing myeloid cells are required to maintain healthy myelinated axons throughout aging and adulthood (Lasiene et al., 2009). However, previous studies have shown that myelin turnover is impacted by the aging process. Human studies estimate length of total myelinated axons is reduced by 27%–45% depending on brain region in old age (Pakkenberg et al., 2003; Peters and Sethares, 2002; Tang et al., 1997). These reductions are known to cause cognitive decline in rodents and primates (Feldman and Peters, 1998; Peters et al., 1996; Rivera et al., 2016; Zhan et al., 2014). Furthermore, myelin fragments accumulate throughout aging and the number of myeloid cells interacting with myelin increases (Poliani et al., 2015; Safaiyan et al., 2016). With increasing age, the levels of myelin debris and the number of myelin defects (including ballooning and loosely packed myelin) increase (Feldman and Peters, 1998). Collectively, our data suggest that the WD turns a homeostatic function of myeloid cells into a damaging one, promoting excessive and premature myelin loss leading to cognitive decline before old age.

Myelin-related genes have been previously shown to be differentially expressed in the spinal cord of mice in response to a high-fat diet (Yoon et al., 2016). In this study by Yoon and colleagues, they show that short-term exposure to a high-fat diet led to a loss of myelin-forming cells and an exercise regime prevented this loss and promoted myelinogenesis. This study contrasts with our findings that show that myelin genes are increased in the corpus callosum in WD-fed mice but there is an overall loss of myelin. Exercise prevents the myelin loss. A number of factors could

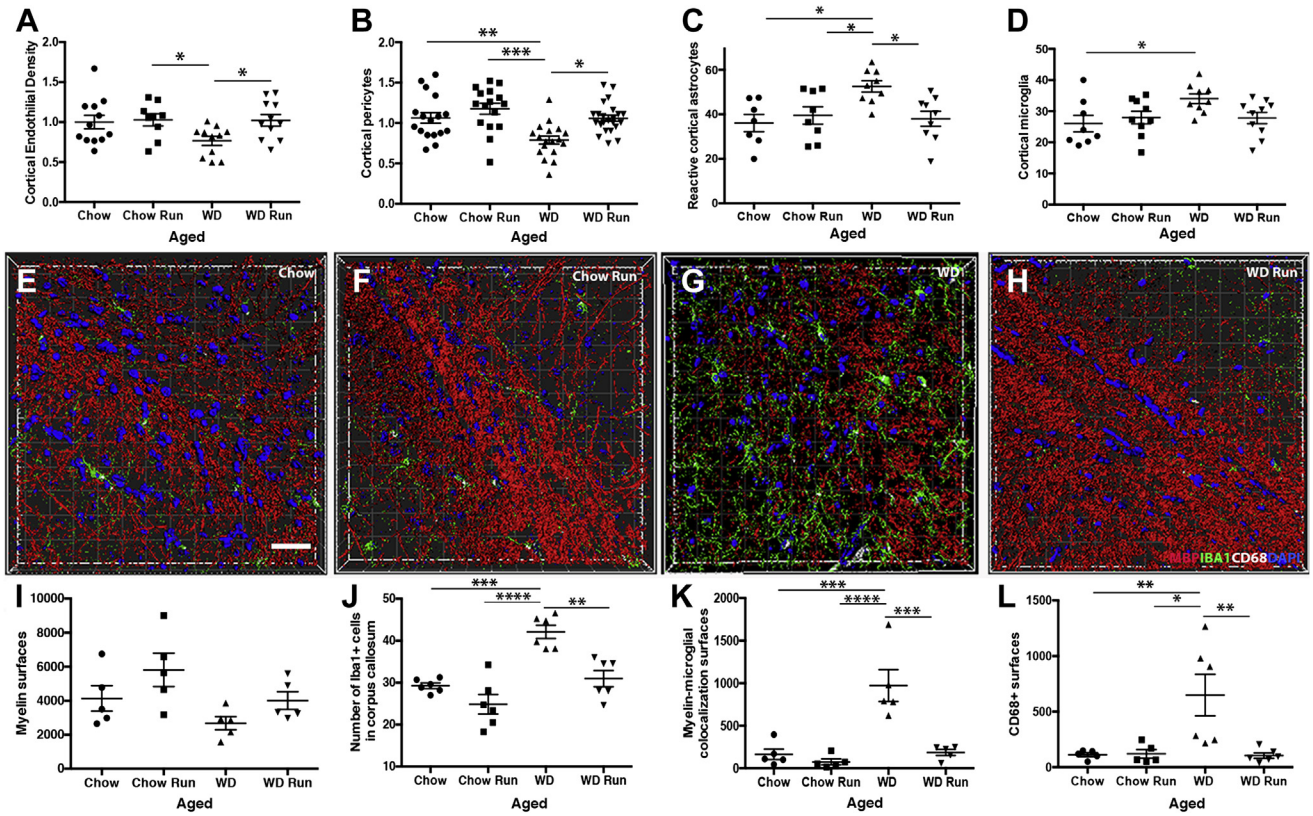

Fig. 8. Running prevents WD-induced cerebrovascular damage and increases in phagocytosing myeloid cells. (A–D) Running prevented WD-induced endothelial cell loss (A, n ≥ 11, chow run vs. sedentary WD $^{*}p = 0.049$, sedentary WD vs. running WD $^{*}p = 0.040$) and the associated decrease in the number of PDGFRβ+ pericytes covering the blood vessels (B, n ≥ 11, sedentary chow vs. sedentary WD $^{**}p = 0.005$, running chow vs. sedentary WD $^{***}p = 0.0007$, sedentary WD vs. running WD $^{*}p = 0.02$). Running also prevented the increase in GFAP+ astrocytes surrounding blood vessels (C, n ≥ 9, sedentary chow vs. sedentary WD $^{*}p = 0.011$, running chow vs. sedentary WD $^{*}p = 0.047$, sedentary WD vs. running WD $^{*}p = 0.018$) and the increase in IBA1+ myeloid cells (D, n ≥ 9, running chow vs. sedentary WD $^{*}p = 0.026$). (E–H) Representative 3D reconstructions of the corpus callosum using IMARIS software of chow sedentary (E), chow run (F), WD sedentary (G), and WD run (H). Images show myelin (MBP, red), DAPI (blue), myeloid cells (IBA1, green), and CD68 (white) to identify phagocytosing myeloid cells. (I–L) Aged running WD mice tended to have more myelin surfaces than aged sedentary WD mice (I). However, in the corpus callosum, running prevented the WD-dependent increase in IBA1+ myeloid cells (J, sedentary chow vs. sedentary WD $^{***}p = 0.0002$, running chow vs. sedentary WD $^{****}p < 0.0001$, sedentary WD vs. running WD $^{**}p = 0.001$), the increase in myelin-myeloid cell interactions (K, sedentary chow vs. sedentary WD $^{***}p = 0.0002$, running chow vs. sedentary WD $^{****}p < 0.0001$, sedentary WD vs. running WD $^{***}p = 0.0003$), and the increase in CD68+ surfaces (L, sedentary chow vs. sedentary WD $^{**}p = 0.01$, running chow vs. sedentary WD $^{*}p = 0.011$, sedentary WD vs. running WD $^{**}p = 0.006$). Scale bar for all images 40 μm.

account for the differences between the 2 studies. Yoon and colleagues used a high-fat diet, whereas ours combines a number of additional features of a westernized diet (Fig. 1; Graham et al., 2016). The previous study also did not assess the effect of a high-fat diet on myeloid cells. Furthermore, the different CNS regions studied (spinal cord compared to brain) may have different requirements or responses to western or high-fat diets.

Given the possible imbalance in myelin turnover, 2 cell types known to be involved in this process, oligodendrocytes (and precursors) and myeloid cells, were assessed. First, transcriptional profiling showed an upregulation of DE genes associated with myelin maintenance by oligodendrocytes, including *Mbp*, *Mag*, and *Plp*, despite our data showing an overall loss of the myelin protein MBP. We also observed an increase in the number of *Plp*-expressing and CC1+ oligodendrocytes in WD-fed mice. The increase in myelin-related genes could be a survival response as oligodendrocyte morphology looks similar between control chow- and WD-fed mice via electron microscopy. In WD-fed mice, despite the myelin appearing ballooned and loosely packed, OLIG2+ oligodendrocytes were aligned within the white matter tracts, suggesting differentiation of oligodendrocytes (Lee et al., 2013; Meyer-Franke et al., 1999; Prayoonwiwat and Rodriguez, 1993). Therefore, based on our data, we propose that the remyelination portion of myelin turnover may still be functioning in WD-fed mice. Second, we tested removal of myelin by myeloid cells. Genes relevant to inflammatory pathways and phagocytosis, including *Cd68*, *Trem2*, and many complement genes were upregulated in both the FPC/corpus callosum and HP of WD fed mice compared to control chow. Previous studies have shown that complement components are necessary for myelin phagocytosis (Brosnan et al., 2013; Domingues et al., 2016; Rutkowski et al., 2010). In addition, in areas of white matter (e.g., corpus callosum), activated, phagocytosing cells pervade these regions and phagocytose myelin ensheathments. In our study, there was a significant increase in interactions between IBA1 (myeloid cell marker) and MBP (myelin protein) "surfaces" (Figs. 6, 8). This analysis included areas where MBP was localized within IBA1 surfaces (indicative of myelin phagocytosis) although MBP inside IBA1 surfaces was not calculated specifically. Further supporting myelin phagocytosis by myeloid cells, many of the IBA1+ cells were also positive for CD68, a commonly used marker of the phagosome. More work is required to determine the precise mechanism(s) by which myelin changes occur in WD-fed mice. However, the increase in genes in the complement cascade in the FPC/CC comparisons (Fig. 1), and previous studies showing the complement cascade is necessary for phagocytosis of synapses, suggest similar mechanisms may be causing phagocytosis of myelin by myeloid cells in obesity.

Young mice fed the WD for only 6 weeks showed cerebrovascular damage and an increase in IBA1+ cells but no evidence of myelin loss. White matter hyperintensities have been identified in areas of astrocyte reactivity and vascular compromise in dementia patients (Fellgiebel et al., 2004; Kalaria, 2010; Zhan et al., 2014). White matter hyperintensities have also been shown in patients with cardiovascular and cerebral small vessel disease (de Leeuw et al., 2001; van Norden et al., 2011). We, and others, have shown previously that astrocyte reactivity occurs in aging and correlates with NVU decline (Montagne et al., 2015; Soto et al., 2015; Zhao et al., 2015) and age-related astrocyte reactivity is exacerbated by the WD (Graham et al., 2016). NVU breakdown and cerebral small vessel disease are known to increase damaging neuroinflammatory responses by macrophages and astrocytes (Del Zoppo, 2009; Fornage et al., 2008; Rouhl et al., 2012; Soto et al., 2015; Yang and Rosenberg, 2011). Given that astrocyte reactivity could directly impact myelin turnover independent of myeloid cell activity (Markoullis et al., 2014; Sharma et al., 2010) and may cause a breakdown in astrocyte-pericyte or astrocyte-endothelial cell interactions leading to cerebrovascular damage (Abbott, 2002; Zhao et al., 2015) targeting astrocyte responses to obesity could provide valuable insights to prevent cerebrovascular and white matter damage and cognitive decline.

The effects of a WD and/or obesity in the context of cognitive aging require more investigation. Midlife obesity has been implicated in increasing risk for age-related cognitive decline and age-related neurodegenerative diseases including many dementias. Many of the changes in the brain that we observed in response to the WD at 12 months (neurovascular changes, increase in astrocyte reactivity, increase in IBA1+ cells) have also been shown at older ages. For instance, we have shown that NVU decline (e.g., loss of pericytes, loss of basement membrane proteins) was apparent in 18–22 months B6 mice fed a normal chow (Soto et al., 2015). These changes correlated with higher numbers of IBA1+ cells suggesting a link between neuroinflammation and neurovascular damage. White matter damage was not assessed in our previous aging study (Soto et al., 2015), and so, a detailed assessment of white matter changes during aging in humans and animal models is still needed. The question remains whether diet/obesity primarily accelerates the aging process or modifies it in synergistic ways. To determine this, more precise assessments of the different cell types in both aging and obesity are required. Data from this study, our (Graham et al., 2016; Soto et al., 2015) and other previous studies (Hong et al., 2016; Shi et al., 2017; Stephan et al., 2013) predict that myeloid cells play an important role in brain health during aging, obesity, and neurodegenerative diseases (reviewed in the study by Newcombe et al., 2018). Myeloid cells include resident microglia, infiltrating monocytes, and macrophages. Recent studies are now identifying subpopulations of resident microglia by single-cell RNA sequencing that change with age (Hammond et al., 2019). Interestingly, 1 study identified a specific population of myeloid cells expressing *Gpnmb* and *Clec7a* that they termed white matter associated microglia (Li et al., 2018). They align with oligodendrocytes during development and brain maturation but aging tissue was not assessed. Similar single-cell profiling approaches can be used to determine how populations of myeloid cells change with diet. Our assessment of myelin phagocytosis by myeloid cells is similar to previous studies that show phagocytosis of synapses by myeloid cells in aging and in neurodegenerative diseases such as Alzheimer's disease. This process is mediated by multiple pathways including the complement cascade. For instance, deletion of *C1qa* and *C3*, key components of the complement cascade improve cognitive aging and prevent synapse loss in mouse models of Alzheimer's disease (Hong et al., 2016; Shi et al., 2017; Stephan et al., 2013). In our transcriptional profiling data, we observed a significant enrichment of genes in the complement cascade in both the HP and FPC/CC comparing aged WD to young chow mice. These data suggest that activation of the complement cascade during aging is exacerbated by chronic consumption of a WD. To date, the role of the complement cascade in diet-induced white matter damage or in diet-induced and age-related neurovascular decline has not been assessed.

Our study showed that exercise, independent of total weight loss, prevented many of the damaging effects of a WD. Voluntary running was able to prevent WD-induced memory deficits measured in 2 separate assays. However, future studies evaluating learning and longer-term memory will be required as the current set of short-term memory tests did not have the sophistication beyond evaluating intact versus impaired short-term memory. Prevention of short-term memory deficits by running correlated with a preservation of white matter damage and neuroinflammation in WD mice. For instance, running prevented the increase in interactions between MBP and IBA1, and the increase in CD68+ cells that were observed after chronic consumption of a WD (Fig. 8). This supports our model that the white matter damage due to excess phagocytosis of myelin by myeloid cells is prevented by running. The precise mechanisms by which exercise prevents diet-induced damage are not clear. However, it is likely that exercise acts in multiple ways to counter the damaging effects of a WD and midlife obesity. A recent study showed that exercise moderates high-fat diet–induced oligodendrocyte death that is seen in adult spinal cord. Previous studies from our laboratory and others have documented the benefits of exercise on age-dependent NVU decline, neurogenesis, cerebral blood flow, and cognition (Gibbons et al., 2014; Nokia et al., 2016; Soto et al., 2015). Cardiovascular risks associated with obesity are significantly reduced in response to exercise. Exercise has also been shown to improve blood flow and angiogenesis in the brain as well as reducing systemic inflammation (Bolduc et al., 2013; Lavie et al., 2011; Swain et al., 2003). Studies have also demonstrated that exercise upregulates neurotrophic factors, such as BDNF, in activity-sensing neurons (Alomari et al., 2013; Vaynman et al., 2004). It is likely that exercise protects the brain through a myriad of factors. Identifying these factors that modify neuroinflammation and prevent neurovascular decline and white matter damage may lead to new combinatorial treatments that protect the brain from the damaging effects of chronic consumption of a WD.

Disclosure

The authors declare no competing interests.

Acknowledgements

The authors thank Drs. Simon John, Mimi DeVries, and Jeffrey Harder for western diet development; Keating Pepper for help with IMARIS; Laura Anderson for behavioral phenotyping; Zoe Reifsnyder for figure development; and John West and Yu-Chien Wu for help with the imaging analysis. This work was funded in part by RF1AG051496 (GRH), The Jane B. Cook Foundation, The Jackson Laboratory Nathan Shock Center of Excellence in the Basic Biology of Aging, National Institute on Aging (K01 AG049050, P30 AG10133, and R01 AG19771), the Alzheimer's Association, the Indiana University Health–Indiana University School of Medicine Strategic Research Initiative, and the Indiana Clinical and Translational Science Institute (CTSI).

Data collection and sharing for this project was funded by the Alzheimer's Disease Neuroimaging Initiative (ADNI) (National Institutes of Health Grant U01 AG024904) and DOD ADNI (Department of Defense award number W81XWH-12-2-0012). ADNI is

funded by the National Institute on Aging, the National Institute of Biomedical Imaging and Bioengineering, and through generous contributions from the following: AbbVie, Alzheimer's Association; Alzheimer's Drug Discovery Foundation; Araclon Biotech; BioClinica, Inc; Biogen; Bristol-Myers Squibb Company; CereSpir, Inc; Cogstate; Eisai Inc; Elan Pharmaceuticals, Inc; Eli Lilly and Company; Euroimmun; F. Hoffmann-La Roche Ltd and its affiliated company Genentech, Inc; Fujirebio; GE Healthcare; IXICO Ltd; Janssen Alzheimer Immunotherapy Research & Development, LLC.; Johnson & Johnson Pharmaceutical Research & Development LLC.; Lumosity; Lundbeck; Merck & Co, Inc; Meso Scale Diagnostics, LLC.; NeuroRx Research; Neurotrack Technologies; Novartis Pharmaceuticals Corporation; Pfizer Inc; Piramal Imaging; Servier; Takeda Pharmaceutical Company; and Transition Therapeutics. The Canadian Institutes of Health Research is providing funds to support ADNI clinical sites in Canada. Private sector contributions are facilitated by the Foundation for the National Institutes of Health (www.fnih.org). The grantee organization is the Northern California Institute for Research and Education, and the study is coordinated by the Alzheimer's Therapeutic Research Institute at the University of Southern California. ADNI data are disseminated by the Laboratory for Neuro Imaging at the University of Southern California.

The datasets generated during and/or analyzed during the present study are available from the corresponding author on reasonable request. All transcriptional profiling data will be submitted to Geo Archives.

Authors' contributions: LCG and GRH conceived the project. LCG, WAG, and YC performed all the experiments with the exception of the behavioral tests which were performed in The Jackson Laboratory's Mouse Neurobehavioral Phenotyping Facility under the direction of SJSR. SJSR developed the experimental design for the behavioral studies with LCG and GRH and analyzed the behavioral data. VMP performed all gene expression analysis. LCG and GRH performed gene set enrichment analyses. SLR performed all human data analysis with additional guidance from AJS. LCG and GRH wrote the manuscript and all authors reviewed and approved the final version.

Appendix A. Supplementary data

Supplementary data to this article can be found online at https://doi.org/10.1016/j.neurobiolaging.2019.03.018.

References

Abbott, N.J., 2002. Astrocyte–endothelial interactions and blood–brain barrier permeability. J. Anat. 200, 523–534.
Ahn, M., Lee, J., Gustafsson, A., Enriquez, A., Lancaster, E., Sul, J.Y., Haydon, P.G., Paul, D.L., Huang, Y., Abrams, C.K., 2008. Cx29 and Cx32, two connexins expressed by myelinating glia, do not interact and are functionally distinct. J. Neurosci. Res. 86, 992–1006.
Ainger, K., Avossa, D., Diana, A.S., Barry, C., Barbarese, E., Carson, J.H., 1997. Transport and localization elements in myelin basic protein mRNA. J. Cell. Biol. 138, 1077–1087.
Alexander, A.L., Lee, J.E., Lazar, M., Field, A.S., 2007. Diffusion tensor imaging of the brain. Neurotherapeutics 4, 316–329.
Alomari, M.A., Khabour, O.F., Alzoubi, K.H., Alzubi, M.A., 2013. Forced and voluntary exercises equally improve spatial learning and memory and hippocampal BDNF levels. Behav. Brain Res. 247, 34–39.
Bell, R.D., Winkler, E.A., Sagare, A.P., Singh, I., LaRue, B., Deane, R., Zlokovic, B.V., 2010. Pericytes control key neurovascular functions and neuronal phenotype in the adult brain and during aging. Neuron 68, 409–427.
Bolduc, V., Thorin-Trescases, N., Thorin, E., 2013. Endothelium-dependent control of cerebrovascular functions through age: exercise for healthy cerebrovascular aging. Am. J. Physiol.Heart Circ. Physiol. 305, H620–H633.
Bolzenius, J.D., Laidlaw, D.H., Cabeen, R.P., Conturo, T.E., McMichael, A.R., Lane, E.M., Heaps, J.M., Salminen, L.E., Baker, L.M., Scott, S.E., Cooley, S.A., Gunstad, J., Paul, R.H., 2015. Brain structure and cognitive correlates of body mass index in healthy older adults. Behav. Brain Res. 278, 342–347.
Broestl, L., Worden, K., Moreno, A.J., Davis, E.J., Wang, D., Garay, B., Singh, T., Verret, L., Palop, J.J., Dubal, D.B., 2018. Ovarian cycle stages modulate Alzheimer-related cognitive and brain Network alterations in female mice. eNeuro 5, 1–18.
Brosnan, C.F., Wul, E., Selmaj, K.W., 2013. Astrocyte/oligodendrocyte interaction in association with reactive gliosis. Biol. Pathol. Astrocyte-Neuron Interactions 2, 395.
Cai, J., Zhu, Q., Zheng, K., Li, H., Qi, Y., Cao, Q., Qiu, M., 2010. Co-localization of Nkx6. 2 and Nkx2. 2 homeodomain proteins in differentiated myelinating oligodendrocytes. Glia 58, 458–468.
Calabro, P., Golia, E., Maddaloni, V., Limongelli, G., Ziello, B., Fimiani, F., Jane Romano, I., Crisci, M., Russo, M.G., Yeh, E.T.H., Calabro, R., 2013. In: Obesity, Inflammation, and Vascular Disease: Novel Insight in the Role of Adipose Tissue, Metabolic Syndrome and Neurological Disorders. John Wiley & Sons Ltd, Hoboken, New Jersey, pp. 311–326.
Campbell II, T.M., 2004. The China Study: The Most Comprehensive Study of Nutrition Ever Conducted and the Startling Implications for Diet, Weight Loss and Long-Term Health. BenBella Books, Inc, Dallas, Texas.
Cecchini, M., Sassi, F., Lauer, J.A., Lee, Y.Y., Guajardo-Barron, V., Chisholm, D., 2010. Tackling of unhealthy diets, physical inactivity, and obesity: health effects and cost-effectiveness. Lancet 376, 1775–1784.
Chakraborty, T.R., Donthireddy, L., Adhikary, D., Chakraborty, S., 2016. Long-term high fat diet has a profound effect on body weight, hormone levels, and estrous cycle in mice. Med. Sci. Monit. 22, 1601–1608.
Chomiak, T., Hu, B., 2009. What is the optimal value of the g-ratio for myelinated fibers in the rat CNS? A theoretical approach. PLoS One 4, e7754.
Colcombe, S.J., Erickson, K.I., Raz, N., Webb, A.G., Cohen, N.J., McAuley, E., Kramer, A.F., 2003. Aerobic fitness reduces brain tissue loss in aging humans. J. Gerontol. A: Biol. Sci. Med. Sci. 58, M176–M180.
Cordain, L., Eaton, S.B., Sebastian, A., Mann, N., Lindeberg, S., Watkins, B.A., O'Keefe, J.H., Brand-Miller, J., 2005. Origins and evolution of the Western diet: health implications for the 21st century. Am. J. Clin. Nutr. 81, 341–354.
Cournot, M., Marquie, J.C., Ansiau, D., Martinaud, C., Fonds, H., Ferrieres, J., Ruidavets, J.B., 2006. Relation between body mass index and cognitive function in healthy middle-aged men and women. Neurology 67, 1208–1214.
de Leeuw, F.E., de Groot, J.C., Achten, E., Oudkerk, M., Ramos, L.M., Heijboer, R., Hofman, A., Jolles, J., van Gijn, J., Breteler, M.M., 2001. Prevalence of cerebral white matter lesions in elderly people: a population based magnetic resonance imaging study. The Rotterdam Scan Study. J. Neurol. Neurosurg. Psychiatry 70, 9–14.
Deacon, R., 2012. Assessing burrowing, nest construction, and hoarding in mice. J. Vis. Exp. 59, e2607.
Del Zoppo, G.J., 2009. Inflammation and the neurovascular unit in the setting of focal cerebral ischemia. Neuroscience 158, 972–982.
Dishman, R.K., Berthoud, H.R., Booth, F.W., Cotman, C.W., Edgerton, V.R., Fleshner, M.R., Gandevia, S.C., Gomez-Pinilla, F., Greenwood, B.N., Hillman, C.H., 2006. Neurobiology of exercise. Obesity 14, 345–356.
Domingues, H.S., Portugal, C.C., Socodato, R., Relvas, J.B., 2016. Oligodendrocyte, astrocyte, and microglia crosstalk in myelin development, damage, and repair. Front. Cell Dev. Biol. 4, 71.
Duncan, G.E., Perri, M.G., Theriaque, D.W., Hutson, A.D., Eckel, R.H., Stacpoole, P.W., 2003. Exercise training, without weight loss, increases insulin sensitivity and postheparin plasma lipase activity in previously sedentary adults. Diabetes Care 26, 557–562.
Elias, M.F., Elias, P.K., Sullivan, L.M., Wolf, P.A., D'Agostino, R.B., 2005. Obesity, diabetes and cognitive deficit: the framingham heart study. Neurobiol. Aging 26 (Supplement), 11–16.
Feldman, M.L., Peters, A., 1998. Ballooning of myelin sheaths in normally aged macaques. J. Neurocytol. 27, 605–614.
Fellgiebel, A., Wille, P., Müller, M.J., Winterer, G., Scheurich, A., Vucurevic, G., Schmidt, L.G., Stoeter, P., 2004. Ultrastructural hippocampal and white matter alterations in mild cognitive impairment: a diffusion tensor imaging study. Dement. Geriatr. Cogn. Disord. 18, 101–108.
Flurkey, K., Currer, J.M., Harrison, D., 2007. In: second ed. Mouse Models in Aging Research, the Mouse in Biomedical Research. Elsevier, Amsterdam, Netherlands, pp. 637–672.
Fornage, M., Chiang, Y.A., O'Meara, E.S., Psaty, B.M., Reiner, A.P., Siscovick, D.S., Tracy, R.P., Longstreth, W., 2008. Biomarkers of inflammation and MRI-defined small vessel disease of the brain the cardiovascular health study. Stroke 39, 1952–1959.
Franciosi, S., De Gasperi, R., Dickstein, D.L., English, D.F., Rocher, A.B., Janssen, W.G., Christoffel, D., Sosa, M.A., Hof, P.R., Buxbaum, J.D., 2007. Pepsin pretreatment allows collagen IV immunostaining of blood vessels in adult mouse brain. J. Neurosci. Methods 163, 76–82.
Fumagalli, M., Daniele, S., Lecca, D., Lee, P.R., Parravicini, C., Fields, R.D., Rosa, P., Antonucci, F., Verderio, C., Trincavelli, M.L., 2011. Phenotypic changes, signaling pathway, and functional correlates of GPR17-expressing neural precursor cells during oligodendrocyte differentiation. J. Biol. Chem. 286, 10593–10604.
Gaesser, G., Angadi, S., Sawyer, B.J., Tucker, W.J., Jarrett, C., 2014. Exercise and Diet Improve Cardiometabolic Risk in Overweight and Obese Individuals without Weight Loss. Elsevier Inc, Amsterdam, Netherlands.
Gibbons, T.E., Pence, B.D., Petr, G., Ossyra, J.M., Mach, H.C., Bhattacharya, T.K., Perez, S., Martin, S.A., McCusker, R.H., Kelley, K.W., 2014. Voluntary wheel running, but not a diet containing (−)-epigallocatechin-3-gallate and β-alanine, improves learning, memory and hippocampal neurogenesis in aged mice. Behav. Brain Res. 272, 131–140.

Glisky, E.L., 2007. Changes in cognitive function in human aging. In: Riddle, D.R. (Ed.), Brain Aging: Models, Methods, and Mechanisms. Chapter 1, Frontiers in Neuroscience. CRC Press/Taylor & Francis, Boca Raton (FL).
Graham, L.C., Harder, J.M., Soto, I., de Vries, W.N., John, S.W.M., Howell, G.R., 2016. Chronic consumption of a western diet induces robust glial activation in aging mice and in a mouse model of Alzheimer's disease. Sci. Rep. 6, 21568.
Grammas, P., Ghatreh-Samany, P., Thirmangalakudi, L., 2006. Thrombin and Inflammatory proteins are elevated in Alzheimer's disease microvessels: implications for disease pathogenesis. J. Alzheimers Dis. 9, 51–58.
Grammas, P., Ovase, R., 2001. Inflammatory factors are elevated in brain microvessels in Alzheimer's disease. Neurobiol. Aging 22, 837–842.
Gray, J., Yeo, G.S., Cox, J.J., Morton, J., Adlam, A.-L.R., Keogh, J.M., Yanovski, J.A., El Gharbawy, A., Han, J.C., Tung, Y.L., 2006. Hyperphagia, severe obesity, impaired cognitive function, and hyperactivity associated with functional loss of one copy of the brain-derived neurotrophic factor (BDNF) gene. Diabetes 55, 3366–3371.
Gunstad, J., Paul, R.H., Cohen, R.A., Tate, D.F., Spitznagel, M.B., Gordon, E., 2007. Elevated body mass index is associated with executive dysfunction in otherwise healthy adults. Compr. Psychiatry 48, 57–61.
Hammond, T.R., Dufort, C., Dissing-Olesen, L., Giera, S., Young, A., Wysoker, A., Walker, A.J., Gergits, F., Segel, M., Nemesh, J., Marsh, S.E., Saunders, A., Macosko, E., Ginhoux, F., Chen, J., Franklin, R.J.M., Piao, X., McCarroll, S.A., Stevens, B., 2019. Single-cell RNA sequencing of microglia throughout the mouse lifespan and in the injured brain reveals complex cell-state changes. Immunity 50, 253–271.e6.
Hong, S., Beja-Glasser, V.F., Nfonoyim, B.M., Frouin, A., Li, S., Ramakrishnan, S., Merry, K.M., Shi, Q., Rosenthal, A., Barres, B.A., Lemere, C.A., Selkoe, D.J., Stevens, B., 2016. Complement and microglia mediate early synapse loss in Alzheimer mouse models. Science 352, 712–716.
Howell, G.R., Macalinao, D.G., Sousa, G.L., Walden, M., Soto, I., Kneeland, S.C., Barbay, J.M., King, B.L., Marchant, J.K., Hibbs, M., 2011. Molecular clustering identifies complement and endothelin induction as early events in a mouse model of glaucoma. J. Clin. Invest. 121, 1429–1444.
Iturria-Medina, Y., Sotero, R., Toussaint, P., Mateos-Pérez, J., Evans, A., Alzheimer's Disease Neuroimaging Initiative, 2016. Early role of vascular dysregulation on late-onset Alzheimer/'s disease based on multifactorial data-driven analysis. Nat. Commun. 7, 11934.
Jack Jr., C.R., Bernstein, M.A., Borowski, B.J., Gunter, J.L., Fox, N.C., Thompson, P.M., Schuff, N., Krueger, G., Killiany, R.J., Decarli, C.S., Dale, A.M., Carmichael, O.W., Tosun, D., Weiner, M.W., 2010. Update on the magnetic resonance imaging core of the Alzheimer's disease neuroimaging initiative. Alzheimers Dement. 6, 212–220.
Jagust, W.J., Bandy, D., Chen, K., Foster, N.L., Landau, S.M., Mathis, C.A., Price, J.C., Reiman, E.M., Skovronsky, D., Koeppe, R.A., 2010. The Alzheimer's Disease Neuroimaging Initiative positron emission tomography core. Alzheimers Dement. 6, 221–229.
Kalaria, R.N., 2010. Vascular basis for brain degeneration: faltering controls and risk factors for dementia. Nutr. Rev. 68, S74–S87.
Kanoski, S.E., Davidson, T.L., 2011. Western diet consumption and cognitive impairment: links to hippocampal dysfunction and obesity. Physiol. Behav. 103, 59–68.
Kullmann, S., Callaghan, M.F., Heni, M., Weiskopf, N., Scheffler, K., Häring, H.-U., Fritsche, A., Veit, R., Preissl, H., 2016. Specific white matter tissue microstructure changes associated with obesity. Neuroimage 125, 36–44.
Kullmann, S., Schweizer, F., Veit, R., Fritsche, A., Preissl, H., 2015. Compromised white matter integrity in obesity. Obes. Rev. 16, 273–281.
Langmead, B., Trapnell, C., Pop, M., Salzberg, S.L., 2009. Ultrafast and memory-efficient alignment of short DNA sequences to the human genome. Genome Biol. 10, R25.
Lasiene, J., Matsui, A., Sawa, Y., Wong, F., Horner, P.J., 2009. Age-related myelin dynamics revealed by increased oligodendrogenesis and short internodes. Aging cell 8, 201–213.
Lautenschlager, N.T., Cox, K.L., Flicker, L., Foster, J.K., van Bockxmeer, F.M., Xiao, J., Greenop, K.R., Almeida, O.P., 2008. Effect of physical activity on cognitive function in older adults at risk for Alzheimer disease: a randomized trial. JAMA 300, 1027–1037.
Lavie, C.J., Church, T.S., Milani, R.V., Earnest, C.P., 2011. Impact of physical activity, cardiorespiratory fitness, and exercise training on markers of inflammation. J. Cardiopulm. Rehabil. Prev. 31, 137–145.
Lavie, C.J., Lee, D.-c., Sui, X., Arena, R., O'Keefe, J.H., Church, T.S., Milani, R.V., Blair, S.N., 2015. Effects of Running on Chronic Diseases and Cardiovascular and All-Cause Mortality, Mayo Clinic Proceedings. Elsevier, Amsterdam, Netherlands, pp. 1541–1552.
Lavie, C.J., Milani, R.V., 2004. Prevalence of anxiety in coronary patients with improvement following cardiac rehabilitation and exercise training. Am. J. Cardiol. 93, 336–339.
Lee, S., Chong, S.Y.C., Tuck, S.J., Corey, J.M., Chan, J.R., 2013. A rapid and reproducible assay for modeling myelination by oligodendrocytes using engineered nanofibers. Nat. Protoc. 8, 771–782.
Lee, S., Kuk, J.L., Davidson, L.E., Hudson, R., Kilpatrick, K., Graham, T.E., Ross, R., 2005. Exercise without weight loss is an effective strategy for obesity reduction in obese individuals with and without Type 2 diabetes. J. Appl. Physiol. (1985) 99, 1220–1225.
Li, B., Dewey, C.N., 2011. RSEM: accurate transcript quantification from RNA-Seq data with or without a reference genome. BMC Bioinformatics 12, 1.
Li, Q., Cheng, Z., Zhou, L., Darmanis, S., Neff, N.F., Okamoto, J., Gulati, G., Bennett, M.L., Sun, L.O., Clarke, L.E., Marschallinger, J., Yu, G., Quake, S.R., Wyss-Coray, T., Barres, B.A., 2018. Developmental heterogeneity of microglia and brain myeloid cells revealed by deep single-cell RNA sequencing. Neuron 101, 207–223.e10.
Lie, M.E., Overgaard, A., Mikkelsen, J.D., 2013. Effect of a postnatal high-fat diet exposure on puberty onset, estrous cycle regularity, and kisspeptin expression in female rats. Reprod. Biol. 13, 298–308.
Markoullis, K., Sargiannidou, I., Schiza, N., Roncaroli, F., Reynolds, R., Kleopa, K.A., 2014. Oligodendrocyte gap junction loss and disconnection from reactive astrocytes in multiple sclerosis gray matter. J. Neuropathol. Exp. Neurol. 73, 865–879.
Markowska, A.L., 1999. Sex dimorphisms in the rate of age-related decline in spatial memory: relevance to alterations in the estrous cycle. J. Neurosci. 19, 8122–8133.
Martin-Rodriguez, E., Guillen-Grima, F., Martí, A., Brugos-Larumbe, A., 2015. Comorbidity associated with obesity in a large population: the APNA study. Obes. Res. Clin. Pract. 9, 435–447.
Mattson, M.P., 2012. Energy intake and exercise as determinants of brain health and vulnerability to injury and disease. Cell Metab. 16, 706–722.
Medic, N., Ziauddeen, H., Ersche, K.D., Farooqi, I.S., Bullmore, E.T., Nathan, P.J., Ronan, L., Fletcher, P.C., 2016. Increased body mass index is associated with specific regional alterations in brain structure. Int. J. Obes. (Lond). 40, 1177–1182.
Meyer-Franke, A., Shen, S., Barres, B.A., 1999. Astrocytes induce oligodendrocyte processes to align with and adhere to axons. Mol. Cell Neurosci. 14, 385–397.
Mizisin, A.P., Nelson, R.W., Sturges, B., Vernau, K.M., LeCouteur, R.A., Williams, D.C., Burgers, M.L., Shelton, G.D., 2007. Comparable myelinated nerve pathology in feline and human diabetes mellitus. Acta Neuropathol. 113, 431–442.
Montagne, A., Barnes, S.R., Sweeney, M.D., Halliday, M.R., Sagare, A.P., Zhao, Z., Toga, A.W., Jacobs, R.E., Liu, C.Y., Amezcua, L., Harrington, M.G., Chui, H.C., Law, M., Zlokovic, B.V., 2015. Blood-brain barrier breakdown in the aging human Hippocampus. Neuron 85, 296–302.
Naderali, E.K., Ratcliffe, S.H., Dale, M.C., 2009. Review: obesity and Alzheimer's disease: a link between body weight and cognitive function in old age. Am. J. Alzheimers Dis. Other Demen. 24, 445–449.
Newcombe, E.A., Camats-Perna, J., Silva, M.L., Valmas, N., Huat, T.J., Medeiros, R., 2018. Inflammation: the link between comorbidities, genetics, and Alzheimer's disease. J. Neuroinflammation. 15, 276.
Nguyen, J.C., Killcross, A.S., Jenkins, T.A., 2014. Obesity and cognitive decline: role of inflammation and vascular changes. Front Neurosci. 8, 375.
Nimmerjahn, A., Kirchhoff, F., Helmchen, F., 2005. Resting microglial cells are highly dynamic surveillants of brain parenchyma in vivo. Science 308, 1314–1318.
Nokia, M.S., Lensu, S., Ahtiainen, J.P., Johansson, P.P., Koch, L.G., Britton, S.L., Kainulainen, H., 2016. Physical exercise increases adult hippocampal neurogenesis in male rats provided it is aerobic and sustained. J. Physiol. 594, 1855–1873.
Norton, S., Matthews, F.E., Barnes, D.E., Yaffe, K., Brayne, C., 2014. Potential for primary prevention of Alzheimer's disease: an analysis of population-based data. Lancet Neurol. 13, 788–794.
Orthmann-Murphy, J.L., Abrams, C.K., Scherer, S.S., 2008. Gap junctions couple astrocytes and oligodendrocytes. J. Mol. Neurosci. 35, 101–116.
Pakkenberg, B., Pelvig, D., Marner, L., Bundgaard, M.J., Gundersen, H.J.G., Nyengaard, J.R., Regeur, L., 2003. Aging and the human neocortex. Exp. Gerontol. 38, 95–99.
Papageorgiou, I., Astrakas, L.G., Xydis, V., Alexiou, G.A., Bargiotas, P., Tzarouchi, L., Zikou, A.K., Kiortsis, D.N., Argyropoulou, M.I., 2017. Abnormalities of brain neural circuits related to obesity: a Diffusion Tensor Imaging study. Magn. Reson. Imaging 37, 116–121.
Patel, R.K., Jain, M., 2012. NGS QC Toolkit: a toolkit for quality control of next generation sequencing data. PLoS One 7, e30619.
Peters, A., 2009. The effects of normal aging on myelinated nerve fibers in monkey central nervous system. Front. Neuroanat. 3, 11.
Peters, A., Rosene, D.L., Moss, M.B., Kemper, T.L., Abraham, C.R., Tigges, J., Albert, M.S., 1996. Neurobiological bases of age-related cognitive decline in the rhesus monkey. J. Neuropathol. Exp. Neurol. 55, 861–874.
Peters, A., Sethares, C., 2002. Aging and the myelinated fibers in prefrontal cortex and corpus callosum of the monkey. J. Comp. Neurol. 442, 277–291.
Petersen, R.C., Aisen, P.S., Beckett, L.A., Donohue, M.C., Gamst, A.C., Harvey, D.J., Jack Jr., C.R., Jagust, W.J., Shaw, L.M., Toga, A.W., Trojanowski, J.Q., Weiner, M.W., 2010. Alzheimer's disease neuroimaging initiative (ADNI): clinical characterization. Neurology 74, 201–209.
Pistell, P.J., Morrison, C.D., Gupta, S., Knight, A.G., Keller, J.N., Ingram, D.K., Bruce-Keller, A.J., 2010. Cognitive impairment following high fat diet consumption is associated with brain inflammation. J. Neuroimmunol. 219, 25–32.
Poliani, P.L., Wang, Y., Fontana, E., Robinette, M.L., Yamanishi, Y., Gilfillan, S., Colonna, M., 2015. TREM2 sustains microglial expansion during aging and response to demyelination. J. Clin. Invest. 125, 2161–2170.
Prayoonwiwat, N., Rodriguez, M., 1993. The potential for oligodendrocyte proliferation during demyelinating disease. J. Neuropathol. Exp. Neurol. 52, 55–63.
Rivera, A., Vanzuli, I., Julio Rodríguez Arellano, J., Butt, A., 2016. Decreased regenerative capacity of oligodendrocyte progenitor cells (NG2-glia) in the ageing brain: a vicious cycle of synaptic dysfunction, myelin loss and neuronal disruption? Curr. Alzheimer Res. 13, 413–418.
Robinson, M.D., McCarthy, D.J., Smyth, G.K., 2010. edgeR: a Bioconductor package for differential expression analysis of digital gene expression data. Bioinformatics 26, 139–140.

Rouhl, R.P., Damoiseaux, J.G., Lodder, J., Theunissen, R.O., Knottnerus, I.L., Staals, J., Henskens, L.H., Kroon, A.A., de Leeuw, P.W., Tervaert, J.W., 2012. Vascular inflammation in cerebral small vessel disease. Neurobiol. Aging 33, 1800–1806.
Rovio, S., Spulber, G., Nieminen, L.J., Niskanen, E., Winblad, B., Tuomilehto, J., Nissinen, A., Soininen, H., Kivipelto, M., 2010. The effect of midlife physical activity on structural brain changes in the elderly. Neurobiol. Aging 31, 1927–1936.
Ruegsegger, G.N., Toedebusch, R.G., Braselton, J.F., Roberts, C.K., Booth, F.W., 2015. Reduced metabolic disease risk profile by voluntary wheel running accompanying juvenile Western diet in rats bred for high and low voluntary exercise. Physiol. Behav. 152, 47–55.
Rushton, W.A.H., 1951. A theory of the effects of fibre size in medullated nerve. J. Physiol. 115, 101–122.
Rutkowski, M.J., Sughrue, M.E., Kane, A.J., Mills, S.A., Fang, S., Parsa, A.T., 2010. Complement and the central nervous system: emerging roles in development, protection and regeneration. Immunol. Cell Biol 88, 781–786.
Safaiyan, S., Kannaiyan, N., Snaidero, N., Brioschi, S., Biber, K., Yona, S., Edinger, A.L., Jung, S., Rossner, M.J., Simons, M., 2016. Age-related myelin degradation burdens the clearance function of microglia during aging. Nat. Neurosci. 19, 995–998.
Sargiannidou, I., Vavlitou, N., Aristodemou, S., Hadjisavvas, A., Kyriacou, K., Scherer, S.S., Kleopa, K.A., 2009. Connexin32 mutations cause loss of function in Schwann cells and oligodendrocytes leading to PNS and CNS myelination defects. J. Neurosci. 29, 4736–4749.
Saykin, A.J., Shen, L., Foroud, T.M., Potkin, S.G., Swaminathan, S., Kim, S., Risacher, S.L., Nho, K., Huentelman, M.J., Craig, D.W., Thompson, P.M., Stein, J.L., Moore, J.H., Farrer, L.A., Green, R.C., Bertram, L., Jack Jr., C.R., Weiner, M.W., 2010. Alzheimer's Disease Neuroimaging Initiative biomarkers as quantitative phenotypes: genetics core aims, progress, and plans. Alzheimers Dement. 6, 265–273.
Sharma, R., Fischer, M.-T., Bauer, J., Felts, P.A., Smith, K.J., Misu, T., Fujihara, K., Bradl, M., Lassmann, H., 2010. Inflammation induced by innate immunity in the central nervous system leads to primary astrocyte dysfunction followed by demyelination. Acta Neuropathol. 120, 223–236.
Shi, Q., Chowdhury, S., Ma, R., Le, K.X., Hong, S., Caldarone, B.J., Stevens, B., Lemere, C.A., 2017. Complement C3 deficiency protects against neurodegeneration in aged plaque-rich APP/PS1 mice. Sci. Transl Med. 9, 1–14.
Smith, K.B., Smith, M.S., 2016. Obesity statistics. Prim. Care 43, 121–135.
Smith, S.M., 2002. Fast robust automated brain extraction. Hum. Brain Mapp. 17, 143–155.
Smith, S.M., Jenkinson, M., Johansen-Berg, H., Rueckert, D., Nichols, T.E., Mackay, C.E., Watkins, K.E., Ciccarelli, O., Cader, M.Z., Matthews, P.M., Behrens, T.E., 2006. Tract-based spatial statistics: voxelwise analysis of multi-subject diffusion data. Neuroimage 31, 1487–1505.
Song, S.K., Sun, S.W., Ramsbottom, M.J., Chang, C., Russell, J., Cross, A.H., 2002. Dysmyelination revealed through MRI as increased radial (but unchanged axial) diffusion of water. Neuroimage 17, 1429–1436.
Soto, I., Grabowska, W.A., Onos, K.D., Graham, L.C., Jackson, H.M., Simeone, S.N., Howell, G.R., 2016. Meox2 haploinsufficiency increases neuronal cell loss in a mouse model of Alzheimer's disease. Neurobiol. Aging 42, 50–60.
Soto, I., Graham, L.C., Richter, H.J., Simeone, S.N., Radell, J.E., Grabowska, W., Funkhouser, W.K., Howell, M.C., Howell, G.R., 2015. APOE stabilization by exercise prevents aging neurovascular dysfunction and complement induction. PLoS Biol. 13, e1002279.
Spieker, E.A., Pyzocha, N., 2016. Economic impact of obesity. Prim. Care 43, 83–95.
Stanek, K.M., Grieve, S.M., Brickman, A.M., Korgaonkar, M.S., Paul, R.H., Cohen, R.A., Gunstad, J.J., 2011. Obesity is associated with reduced white matter integrity in otherwise healthy adults*. Obesity 19, 500–504.
Stephan, A.H., Madison, D.V., Mateos, J.M., Fraser, D.A., Lovelett, E.A., Coutellier, L., Kim, L., Tsai, H.H., Huang, E.J., Rowitch, D.H., Berns, D.S., Tenner, A.J., Shamloo, M., Barres, B.A., 2013. A dramatic increase of C1q protein in the CNS during normal aging. J. Neurosci. 33, 13460–13474.
Sternberger, N.H., Itoyama, Y., Kies, M.W., Webster, H.deF., 1978. Immunocytochemical method to identify basic protein in myelin-forming oligodendrocytes of newborn rat CNS. J. Neurocytol. 7, 251–263.
Sukoff Rizzo, S.J., Anderson, L.C., Green, T.L., McGarr, T., Wells, G., Winter, S.S., 2018. Assessing healthspan and lifespan measures in aging mice: optimization of testing protocols, replicability, and rater reliability. Curr. Protoc. Mouse Biol. 8, e45.
Swain, R.A., Harris, A.B., Wiener, E.C., Dutka, M.V., Morris, H.D., Theien, B.E., Konda, S., Engberg, K., Lauterbur, P.C., Greenough, W.T., 2003. Prolonged exercise induces angiogenesis and increases cerebral blood volume in primary motor cortex of the rat. Neuroscience 117, 1037–1046.
Tang, Y., Nyengaard, J.R., Pakkenberg, B., Gundersen, H.J., 1997. Age-induced white matter changes in the human brain: a stereological investigation. Neurobiol. Aging 18, 609–615.
Trojanowski, J.Q., Vandeerstichele, H., Korecka, M., Clark, C.M., Aisen, P.S., Petersen, R.C., Blennow, K., Soares, H., Simon, A., Lewczuk, P., Dean, R., Siemers, E., Potter, W.Z., Weiner, M.W., Jack Jr., C.R., Jagust, W., Toga, A.W., Lee, V.M., Shaw, L.M., 2010. Update on the biomarker core of the Alzheimer's disease neuroimaging initiative subjects. Alzheimers Dement. 6, 230–238.
Tucsek, Z., Toth, P., Tarantini, S., Sosnowska, D., Gautam, T., Warrington, J.P., Giles, C.B., Wren, J.D., Koller, A., Ballabh, P., Sonntag, W.E., Ungvari, Z., Csiszar, A., 2014. Aging exacerbates obesity-induced cerebromicrovascular rarefaction, neurovascular uncoupling, and cognitive decline in mice. J. Gerontol. A. Biol. Sci. Med. Sci. 69, 1339–1352.
Turken, Whitfield-Gabrieli, S., Bammer, R., Baldo, J., Dronkers, N.F., Gabrieli, J.D.E., 2008. Cognitive processing speed and the structure of white matter pathways: convergent evidence from normal variation and lesion studies. Neuroimage 42, 1032–1044.
Valladolid-Acebes, I., Stucchi, P., Cano, V., Fernández-Alfonso, M., Merino, B., Gil-Ortega, M., Fole, A., Morales, L., Ruiz-Gayo, M., Del Olmo, N., 2011. High-fat diets impair spatial learning in the radial-arm maze in mice. Neurobiol. Learn. Mem. 95, 80–85.
van Norden, A.G., de Laat, K.F., Gons, R.A., van Uden, I.W., van Dijk, E.J., van Oudheusden, L.J., Esselink, R.A., Bloem, B.R., van Engelen, B.G., Zwarts, M.J., Tendolkar, I., Olde-Rikkert, M.G., van der Vlugt, M.J., Zwiers, M.P., Norris, D.G., de Leeuw, F.-E., 2011. Causes and consequences of cerebral small vessel disease. The RUN DMC study: a prospective cohort study. Study rationale and protocol. BMC Neurol. 11, 29.
Van Praag, H., Shubert, T., Zhao, C., Gage, F.H., 2005. Exercise enhances learning and hippocampal neurogenesis in aged mice. J. Neurosci. 25, 8680–8685.
Vaynman, S., Ying, Z., Gomez-Pinilla, F., 2004. Hippocampal BDNF mediates the efficacy of exercise on synaptic plasticity and cognition. Eur. J. Neurosci. 20, 2580–2590.
Veit, R., Kullmann, S., Heni, M., Machann, J., Häring, H.-U., Fritsche, A., Preissl, H., 2014. Reduced cortical thickness associated with visceral fat and BMI. Neuroimage Clin. 6, 307–311.
Villareal, D.T., Banks, M., Sinacore, D.R., Siener, C., Klein, S., 2006. Effect of weight loss and exercise on frailty in obese older adults. Arch. Intern. Med. 166, 860–866.
Wasseff, S.K., Scherer, S.S., 2011. Cx32 and Cx47 mediate oligodendrocyte: astrocyte and oligodendrocyte: oligodendrocyte gap junction coupling. Neurobiol. Dis. 42, 506–513.
Weiner, M.W., Aisen, P.S., Jack Jr., C.R., Jagust, W.J., Trojanowski, J.Q., Shaw, L., Saykin, A.J., Morris, J.C., Cairns, N., Beckett, L.A., Toga, A., Green, R., Walter, S., Soares, H., Snyder, P., Siemers, E., Potter, W., Cole, P.E., Schmidt, M., 2010. The Alzheimer's disease neuroimaging initiative: progress report and future plans. Alzheimers Dement. 6, 202–211.e7.
Weiner, M.W., Veitch, D.P., Aisen, P.S., Beckett, L.A., Cairns, N.J., Green, R.C., Harvey, D., Jack, C.R., Jagust, W., Liu, E., Morris, J.C., Petersen, R.C., Saykin, A.J., Schmidt, M.E., Shaw, L., Siuciak, J.A., Soares, H., Toga, A.W., Trojanowski, J.Q., 2012. The Alzheimer's Disease Neuroimaging Initiative: a review of papers published since its inception. Alzheimers Dement. 8 (Supplement), S1–S68.
Williams, P.T., Thompson, P.D., 2013. Walking versus running for hypertension, cholesterol, and diabetes mellitus risk reduction. Arterioscler. Thromb. Vasc. Biol. 33, 1085–1091.
Winkler, A.M., Ridgway, G.R., Webster, M.A., Smith, S.M., Nichols, T.E., 2014. Permutation inference for the general linear model. Neuroimage 92, 381–397.
World Health Organization, 2009. Global Health Risks: Mortality and Burden of Disease Attributable to Selected Major Risks. World Health Organization.
Yang, Y., Rosenberg, G.A., 2011. Blood–brain barrier breakdown in acute and chronic cerebrovascular disease. Stroke 42, 3323–3328.
Yoon, H., Kleven, A., Paulsen, A., Kleppe, L., Wu, J., Ying, Z., Gomez-Pinilla, F., Scarisbrick, I.A., 2016. Interplay between exercise and dietary fat modulates myelinogenesis in the central nervous system. Biochim. Biophys. Acta 1862, 545–555.
Zhan, X., Jickling, G.C., Ander, B.P., Liu, D., Stamova, B., Cox, C., Jin, L.W., DeCarli, C., Sharp, F.R., 2014. Myelin injury and degraded myelin vesicles in Alzheimer's disease. Curr. Alzheimer Res. 11, 232–238.
Zhao, Z., Nelson, A.R., Betsholtz, C., Zlokovic, B.V., 2015. Establishment and dysfunction of the blood-brain barrier. Cell 163, 1064–1078.